



**HAL**  
open science

## Fast inference with Kronecker-sparse matrices

Antoine Gonon, Léon Zheng, Pascal Carrivain, Quoc-Tung Le

► **To cite this version:**

Antoine Gonon, Léon Zheng, Pascal Carrivain, Quoc-Tung Le. Fast inference with Kronecker-sparse matrices. 2024. hal-04584450v2

**HAL Id: hal-04584450**

**<https://hal.science/hal-04584450v2>**

Preprint submitted on 23 May 2024 (v2), last revised 3 Nov 2024 (v4)

**HAL** is a multi-disciplinary open access archive for the deposit and dissemination of scientific research documents, whether they are published or not. The documents may come from teaching and research institutions in France or abroad, or from public or private research centers.

L'archive ouverte pluridisciplinaire **HAL**, est destinée au dépôt et à la diffusion de documents scientifiques de niveau recherche, publiés ou non, émanant des établissements d'enseignement et de recherche français ou étrangers, des laboratoires publics ou privés.

---

# Make Inference Faster: Efficient GPU Memory Management for Butterfly Sparse Matrix Multiplication

---

**Antoine Gonon\***  
Univ Lyon, EnsL, UCBL,  
CNRS, Inria, LIP

**Léon Zheng\***  
valeo.ai,  
Univ Lyon, EnsL, UCBL,  
CNRS, Inria, LIP

**Pascal Carrivain\***  
Univ Lyon, EnsL, UCBL,  
CNRS, Inria, LIP

**Quoc-Tung Le**  
Univ Lyon, EnsL, UCBL,  
CNRS, Inria, LIP

## Abstract

This paper is the first to assess the state of existing sparse matrix multiplication algorithms on GPU for the *butterfly* structure, a promising form of sparsity. This is achieved through a comprehensive benchmark that can be easily modified to add a new implementation. The goal is to provide a simple tool for users to select the optimal implementation based on their settings. Using this benchmark, we find that existing implementations spend up to 50% of their total runtime on memory rewriting operations. We show that these memory operations can be optimized by introducing a new CUDA kernel that minimizes the transfers between the different levels of GPU memory, achieving a median speed-up factor of  $\times 1.4$  while also reducing energy consumption (median of  $\times 0.85$ ). We also demonstrate the broader significance of our results by showing how the new kernel can speed up the inference of neural networks.

## 1 Introduction

Accelerating the inference and training of deep neural networks is a major challenge given their constantly growing resource requirements. At the very heart of this is the acceleration of matrix multiplication on GPU, which is one of the main operation during training and inference. For instance, in a forward pass of vision transformers (ViTs) [Dosovitskiy et al., 2020], between 30% and 60% of the total time is spent in linear layers (see Appendix B.6 for details). One key approach that aims to accelerate computations is by enforcing *sparsity* constraints on certain weight matrices in the model.

The butterfly matrices have emerged as a promising form of sparse matrices: approximating a matrix by a product of butterfly factors can be done using an efficient algorithm that outperforms gradient descent, with some guarantees of reconstruction if the target matrix admits exactly or approximately a butterfly factorization [Le et al., 2022, Zheng et al., 2023, Le, 2023]; butterfly matrices can be quantized more efficiently than by naive rounding [Gribonval et al., 2023]; and butterfly matrices have a nearly linear *theoretical* complexity for matrix-vector multiplication. The latter is precisely why many linear operators, such as the Discrete Fourier Transform (DFT) or the Hadamard Transform, have fast algorithms: they can be written as butterfly matrices, allowing for fast implementations of these operators. This nearly linear *theoretical* complexity for matrix-vector multiplication comes

---

\*Equal contribution

from the definition of a butterfly matrix  $\mathbf{W}$ : it must admits a factorization  $\mathbf{W} = \mathbf{B}_1 \dots \mathbf{B}_L$ , called *butterfly factorization*, where each factor  $\mathbf{B}_\ell$  has some specific *structured* sparsity pattern (support of the matrix) with an associated small theoretical multiplication complexity. In general, the support of a butterfly factor is of the form of  $\mathbf{S}_\pi = \mathbf{I}_a \otimes \mathbf{1}_{b \times c} \otimes \mathbf{I}_d$  (Figure 2) for some tuple of integers  $\pi = (a, b, c, d)$ , where  $\otimes$  denotes the Kronecker product,  $\mathbf{1}_{m \times n}$  is the matrix of size  $m \times n$  full of ones, and  $\mathbf{I}_n$  is the identity matrix of size  $n$ , see Definition 2.1 below [Lin et al., 2021, Le, 2023]. A concrete example is given in Figure 1.

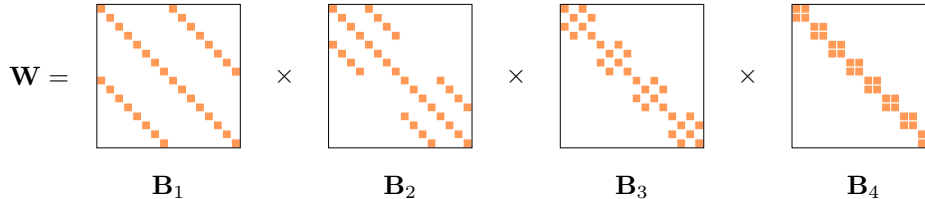


Figure 1: Example of butterfly factorization  $\mathbf{W} = \mathbf{B}_1 \dots \mathbf{B}_L$ , for  $L = 4$ . Here, the factor  $\mathbf{B}_\ell \in \mathbb{R}^{N \times N}$  (with  $N = 2^L$ ) has support  $\mathbf{S}_\ell = \mathbf{I}_{2^{\ell-1}} \otimes \mathbf{1}_{2 \times 2} \otimes \mathbf{I}_{2^{L-\ell}}$ . This corresponds to the butterfly factorization of the Discrete Fourier Transform matrix  $\mathbf{W}$ , up to a permutation of its column indices. In practice, the goal is to replace weight matrices of neural networks by butterfly matrices  $\mathbf{W} = \mathbf{B}_1 \dots \mathbf{B}_L$  while having (i) at least the same accuracy for the learning task at hand, (ii) less parameters to store, and (iii) an accelerated inference and training phase. To the best of our knowledge, previous works mostly focused on (i) and (ii) [Vahid et al., 2020, Lin et al., 2021, Dao et al., 2022a,b]. This paper is the first<sup>2</sup> to extensively study the *time efficiency* of these butterfly networks.

**Main contributions.** (i) The first contribution is to assess for the *first time* the efficiency of many baseline PyTorch GPU implementations for multiplying a batch of vectors with a butterfly matrix, including those that rely on existing efficient routines for batch GEMM<sup>3</sup>, block-sparse matrix multiplication and tensor contraction. The goal is to provide a benchmark that can be easily adapted to include a new implementation, and that can be used to select the best implementation for given settings.

(ii) The existing implementations call high-performance libraries from Python. However, Python lacks routines to explicitly control the GPU memory transfers, and because of that, we find with our benchmark that existing implementations spend up to 50% of their total runtime on GPU memory rewriting operations. To address this, we release a new open-source CUDA kernel that minimizes the transfers between the different levels of GPU memory, achieving a median speed-up factor of  $\times 1.4$  in *float-precision* while also improving energy efficiency with a median reduction factor of  $\times 0.85$ . We further show that the new kernel gets more and more advantageous when the relative number of memory rewrites increases. We also demonstrate the broader significance of our results by showing how the new kernel can accelerate the inference of neural networks.

**Outline.** Section 2 introduces the framework to study butterfly matrix multiplication, and describes baseline GPU implementations on PyTorch. Section 3 assesses for the first time the cost of GPU memory access in these baselines. Section 4 explains how the new CUDA kernel reduces the memory transfer compared to previous existing implementations. Section 5 benchmarks the execution time and the energy consumption of baseline GPU implementations on PyTorch, and the new kernel, for the multiplication with a single butterfly factor. Section 6 concretely illustrates broader implications of this work: the new kernel can be used to speed up the inference of neural networks.

## 2 Background on butterfly factorization

We adopt the definition of butterfly matrices stemming from Lin et al. [2021] and mathematically formalized in Le [2023]. To the best of our knowledge, it captures all the variants of butterfly factorizations that have been empirically tested for deep neural networks in the literature [Dao et al., 2019, 2022a,b, Vahid et al., 2020, Lin et al., 2021, Fu et al., 2023]. Details about this unification are given for the curious readers in Appendix C.2.

<sup>2</sup>See Appendix A for the only numerical reports we found in the literature.

<sup>3</sup>GEMM stands for General Matrix Multiplication.

**Definition 2.1** (Butterfly factor, architecture and matrix). Given a tuple  $\pi := (a, b, c, d) \in (\mathbb{N}_{>0})^4$ , a matrix  $\mathbf{B} \in \mathbb{R}^{abd \times acd}$  is called a  $\pi$ -butterfly factor (or simply *factor* when  $\pi$  is clear from the context) if  $\text{supp}(\mathbf{B}) \subseteq \text{supp}(\mathbf{S}_\pi)$ , where  $\mathbf{S}_\pi := \mathbf{I}_a \otimes \mathbf{1}_{b \times c} \otimes \mathbf{I}_d$  (see Figure 2) and where  $\text{supp}(\mathbf{M})$  denotes the support of a matrix  $\mathbf{M}$ , i.e., the subset of indices  $(i, j)$  for which the entries of  $\mathbf{M}$  at  $(i, j)$  is nonzero. The set of  $\pi$ -butterfly factors is denoted  $\Sigma^\pi$ .

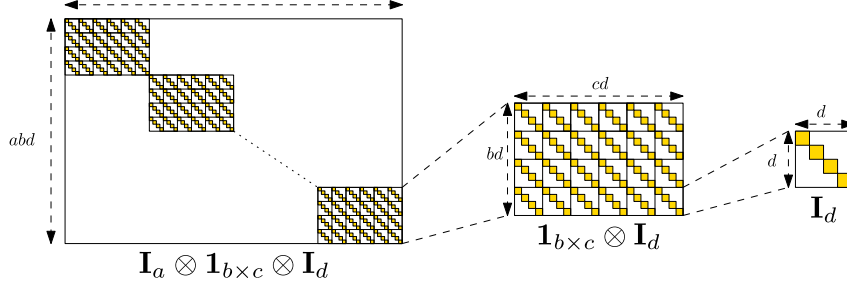


Figure 2: A  $\pi$ -butterfly factor with  $\pi = (a, b, c, d)$  is a block-diagonal matrix with  $a$  blocks, where each block itself is a block matrix composed by  $b \times c$  diagonal matrices of size  $d \times d$ .

A butterfly architecture of depth  $L \in \mathbb{N}_{>0}$  is a sequence  $\beta = (\pi_\ell)_{\ell=1}^L$  of patterns  $\pi_\ell = (a_\ell, b_\ell, c_\ell, d_\ell) \in (\mathbb{N}_{>0})^4$  satisfying the following compatibility condition<sup>4</sup>:  $a_\ell c_\ell d_\ell = a_{\ell+1} b_{\ell+1} d_{\ell+1}$  for  $\ell \in \{1, \dots, L-1\}$ . A matrix  $\mathbf{W}$  is called a butterfly matrix if there exists a butterfly architecture  $\beta = (\pi_\ell)_{\ell=1}^L$  with associated  $\pi_\ell$ -butterfly factors  $\mathbf{B}_\ell$  such that  $\mathbf{W} = \mathbf{B}_1 \dots \mathbf{B}_L$ .

Therefore, a  $\pi$ -butterfly factor is *sparse* and *structured*. It has at most  $abcd$  nonzero entries when  $\pi = (a, b, c, d)$ , which yields a sparsity ratio  $\frac{abcd}{a^2bcd^2} = \frac{1}{ad}$ , since it is of size  $abd \times acd$ .

## 2.1 Generic algorithm for butterfly sparse matrix multiplication

Algorithm 1 is a generic algorithm tailored to the butterfly sparsity, allowing for the multiplication of a batch of vectors with a single  $\pi$ -butterfly factor. It generalizes to general butterfly patterns  $\pi = (a, b, c, d)$  the one suggested by Dao et al. [2022b] in the specific cases  $a = 1$  or  $d = 1$ .

---

### Algorithm 1 Butterfly sparse matrix multiplication

---

**Input:**  $\pi = (a, b, c, d)$ ,  $\mathbf{B} \in \Sigma^\pi$ ,  $\mathbf{X} \in \mathbb{R}^{K \times N}$  ( $N := acd$ )  
**Output:**  $\mathbf{Y} = \mathbf{X}\mathbf{B}^\top \in \mathbb{R}^{K \times M}$  ( $M := abd$ )  
1:  $\mathbf{Y} \leftarrow \mathbf{0}_{K \times M}$   
2: **for**  $(i, j) \in \llbracket 0, a-1 \rrbracket \times \llbracket 0, d-1 \rrbracket$  **do**  
3:    $\text{col} \leftarrow \{i \frac{N}{a} + j + \ell d \mid \ell \in \llbracket 0, c-1 \rrbracket\}$   
4:    $\text{row} \leftarrow \{i \frac{M}{a} + j + kd \mid k \in \llbracket 0, b-1 \rrbracket\}$   
5:    $\mathbf{Y}[:, \text{row}] \leftarrow \mathbf{X}[:, \text{col}] \mathbf{B}^\top[\text{col}, \text{row}]$   
6: **end for**

---



---

### Algorithm 2 Equivalent formulation

---

**Input:**  $\pi$ ,  $\mathbf{X}$ ,  $\tilde{\mathbf{B}} := \mathbf{P}^\top \mathbf{B} \mathbf{Q}^\top$  with  
 $\mathbf{B} \in \Sigma^\pi$ ,  $\mathbf{P} := (\mathbf{I}_a \otimes \mathbf{P}_{b,d})$ ,  
 $\mathbf{Q} := (\mathbf{I}_a \otimes \mathbf{P}_{c,d})^\top$  cf. (1)  
**Output:**  $\mathbf{Y} = \mathbf{X}\mathbf{B}^\top \in \mathbb{R}^{K \times M}$   
1:  $\tilde{\mathbf{X}} \leftarrow \mathbf{X}\mathbf{Q}^\top$   
2:  $\tilde{\mathbf{Y}} \leftarrow \tilde{\mathbf{X}}\tilde{\mathbf{B}}^\top$   
3:  $\mathbf{Y} \leftarrow \tilde{\mathbf{Y}}\mathbf{P}^\top$

---

**Notations.**  $\mathbf{X} \in \mathbb{R}^{K \times N}$  is the input matrix (batch size  $K$ , input dimension  $N$ ).  $\Sigma^\pi$  is the set of matrices with butterfly pattern  $\pi = (a, b, c, d)$  (Definition 2.1).  $\mathbf{0}_{m \times n}$  is the  $m \times n$  matrix filled with zeros. For integers  $a \leq b$ ,  $\llbracket a, b \rrbracket := \{a, a+1, \dots, b\}$ . For a matrix  $\mathbf{M}$ ,  $\mathbf{M}[I, :]$  is the submatrix restricted to rows  $I$ , and  $\mathbf{M}[I, J]$  is the restriction to rows  $I$  and columns  $J$ . Matrix transposition is represented by  $\top$ . Matrix indices start at zero.

**Theoretical complexity.** It is not hard to see that the theoretical complexity of Algorithm 1, defined as the number of scalar multiplications, is  $Kabcd$ , for a batch size  $K$  and a pattern  $\pi = (a, b, c, d)$ .

**On Algorithm 1, and the equivalent Algorithm 2.** When  $d = 1$ , the butterfly factor  $\mathbf{B}$  is block-diagonal with  $a$  dense blocks, as can be seen from Figure 2. In this special case, Algorithm 1 loops over *each of these blocks*, given by  $\mathbf{B}[\text{row}, \text{col}]$ , where the subsets  $\text{row}$  and  $\text{col}$  are indexed by  $i \in \llbracket 0, a-1 \rrbracket$  in Algorithm 1, and performs the matrix multiplication with the corresponding submatrix of  $\mathbf{X}$ . **The general case  $d \geq 1$  is similar: the butterfly factor  $\mathbf{B}$  is, up to permutation**

<sup>4</sup>The compatibility condition ensures that the output dimension of  $\mathbf{B}_{\ell+1}$  matches the input dimension of  $\mathbf{B}_\ell$  so that the product  $\mathbf{B}_1 \dots \mathbf{B}_L$  is well-defined.

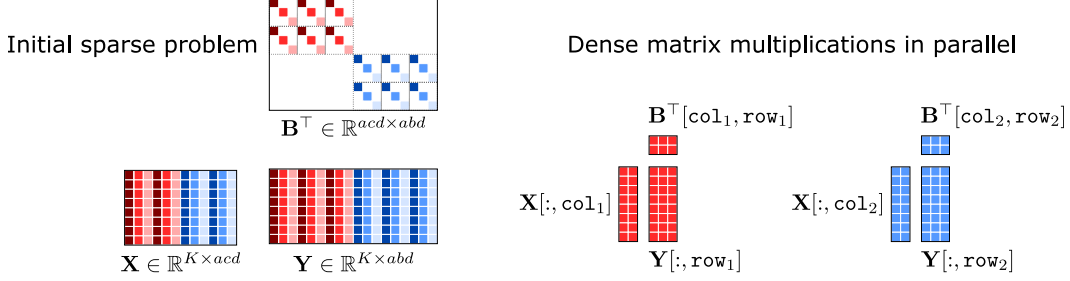


Figure 3: Illustration of Algorithm 1 for sparsity pattern  $\pi = (2, 3, 2, 3)$  and batch size  $K = 8$ . The subsets of rows and columns ( $\text{row}_1, \text{col}_1$ ) are associated with the values  $(i, j) = (0, 1)$  in the “for” loop of Algorithm 1, whereas  $(\text{row}_2, \text{col}_2)$  are associated with  $(i, j) = (1, 1)$ .

operations, block-diagonal with  $ad$  dense blocks, and Algorithm 1 loops over each of these dense blocks, given by  $B[\text{row}, \text{col}]$  with  $\text{row}$  and  $\text{col}$  defined in lines 3 and 4. See Figure 3 for an illustration. More precisely, for any  $\pi = (a, b, c, d)$ , denoting  $\tilde{\pi} = (ad, b, c, 1)$ , we have:

$$S_\pi = \underbrace{(I_a \otimes P_{b,d})}_{:=P} \underbrace{(I_{ad} \otimes \mathbf{1}_{b \times c})}_{:=S_\pi} \underbrace{(I_a \otimes P_{c,d})^\top}_{:=Q} = PS_\pi Q, \quad (1)$$

where  $P_{p,q}$  for two integers  $p, q$  is the so-called  $(p, q)$  perfect shuffle permutation matrix of size  $pq \times pq$  [Van Loan, 2000] (see Appendix C.1 for details). Therefore, for any  $B \in \Sigma^\pi$ , we have  $B = P\tilde{B}Q$  with  $\tilde{B} := P^\top BQ^\top \in \Sigma^{\tilde{\pi}}$ , i.e.,  $\tilde{B}$  is block-diagonal with  $ad$  dense blocks of size  $b \times c$ . Algorithm 1 loops over each of the  $ad$  dense submatrices  $\tilde{B}[\text{row}, \text{col}]$  and accumulates the result in  $\tilde{Y}$ . Many concrete implementations of Algorithm 1 presented below are based on the equivalent formulation  $Y = XB^\top = XQ^\top \tilde{B}^\top P^\top$ : they directly store  $\tilde{B}^\top$  instead of  $B^\top$ , permute the inputs with  $Q$ , multiply with  $\tilde{B}^\top$ , and repermute with  $P$ , which corresponds to Algorithm 2.

## 2.2 Baseline GPU implementations

We now describe concrete baseline GPU implementations of Algorithms 1 and 2. The exact codes are given in Appendix D.1.

**bmm and bsr implementations.** We consider the `bmm` implementation from Dao et al. [2022b], and we also propose a new implementation `bsr`. **Note that the original `bmm` implementation from Dao et al. [2022b] only works for a pattern  $\pi = (a, b, c, d)$  satisfying  $a = 1$  or  $d = 1$ .** We extend it to the general case. Both `bmm` and `bsr` implement Algorithm 2 as specified by Table 1. For the multiplication with  $\tilde{B}$  (line 2 in Algorithm 2), `bmm` relies on batched GEMM NVIDIA routines called through `torch.bmm`, while `bsr` relies on the PyTorch block-sparse library.

	<code>bmm</code>	<code>bsr</code>
Storage format for $\tilde{B}$	3D-tensor of shape $(ad, b, c)$	2D-tensor of shape $(abd, acd)$ stored in BSR <sup>3</sup> format
Line 1 of Algorithm 2	<code>torch.reshape</code>	
Line 2 of Algorithm 2	<code>torch.bmm</code>	<code>torch.nn.functional.linear</code>
Line 3 of Algorithm 2	<code>torch.reshape</code>	

Table 1: Differences in the implementation of Algorithm 2 between `bmm` and `bsr`.

**einsum implementation.** We propose a new baseline implementing Algorithm 1 with tensor contractions, using the `einops` library [Rogozhnikov, 2021]. It stores the nonzero entries of  $B \in \Sigma^\pi$  with a 4D-tensor `B_einsum` of shape  $(a, b, c, d)$ , in such a way that the slice `B_einsum[i, :, :, j]` for  $(i, j) \in \llbracket 0, a-1 \rrbracket \times \llbracket 0, d-1 \rrbracket$  stores the entries of  $B[\text{row}, \text{col}]$  where  $\text{row}, \text{col}$  are defined in lines 3 and 4 of Algorithm 1. The batched matrix multiplication operations at line 5 are then implemented using Einstein summation between this 4D-tensor and a reshaped input tensor.

The above implementations (`bmm`, `bsr`, `einsum`) can be compared to the two following generic implementations (`dense` and `sparse`) that ignore the butterfly sparsity.

**dense implementation.** This ignores the sparsity of the butterfly factor  $B$ , by storing *all* its entries, including zeros, in a tensor of shape  $(M, N)$ . The multiplication is done with `torch.nn.functional.linear`, the default PyTorch implementation for linear layers.

**sparse implementation.** This exploits the sparsity of the butterfly factor  $\mathbf{B}$  but not its structure (recall that the sparsity pattern is not arbitrary, but structured as Kronecker products, see Definition 2.1). The nonzero entries of the factor  $\mathbf{B}$  are saved in a tensor stored in the Compressed Sparse Row (CSR) format, and the matrix multiplication is done with `torch.nn.functional.linear`.

**Batch-size-first vs. batch-size-last.** The entries of the input  $\mathbf{X} \in \mathbb{R}^{K \times N}$  can be stored either in a PyTorch tensor `X_bs1` of shape  $(K, N)$ , or in a PyTorch tensor `X_bs1` of shape  $(N, K)$ , in such a way that the entries of the row  $\mathbf{X}[k, :]$  are stored in the slices `X_bs1[k, :]` and `X_bs1[:, k]`. Because of PyTorch’s row-major convention, the tensor `X_bs1` stores in contiguous memory the entries of each row  $\mathbf{X}[k, :]$ , as opposed to `X_bs1` that store contiguously the entries of each column  $\mathbf{X}[:, i]$ . These two different memory layouts are called *batch-size-first* and *batch-size-last*<sup>6</sup> in this paper. Note that the tensor saving the output  $\mathbf{Y} = \mathbf{X}\mathbf{B}^\top$  will always be in the same memory layout as the input tensor. All the implementations above can be implemented in both ways. While the main point of the paper is to compare the implementations, we will also study the effect of this memory layout convention.

### 3 Memory accesses in baseline implementations

While it is not clear what the tensor contraction `einsum` implementation is exactly doing underneath, the implementations `bmm` and `bsr` explicitly perform permutation operations corresponding to  $\mathbf{P}$  and  $\mathbf{Q}$  (lines 1 and 3 in Algorithm 2) to be able to use high-performance multiplication routines for the multiplication with  $\tilde{\mathbf{B}}$  (line 2 in Algorithm 2). This paper assesses for the first time the cost of these memory operations in practice, as we now discuss.

**Importance of data transfers.** GPU memory management plays a critical role in optimizing performance. Memory in a GPU is organized hierarchically, with global memory being the largest and slowest, followed by shared memory, and finally registers, which are the smallest and fastest [NVIDIA, 2024, Sec. 2.3]. By default, data resides in the global memory of the GPU. Each thread of the GPU runs a kernel that reads data from global memory into registers, performs register-level computations, and writes the results back to global memory. Therefore, when operations are bottlenecked by memory accesses, it is critical to minimize data transfers between global memory, shared memory, and registers to obtain an efficient GPU implementation [NVIDIA, 2024, Sec. 5.3].

**Data transfers in baseline implementations.** In this paper, we argue that the baseline `bmm`, `bsr` and `einsum` implementations for butterfly multiplication require performing *several passes between global memory and registers that can account for a large proportion of the total runtime* in practice. This suggests that there is room for improvement in the memory accesses of these implementations.

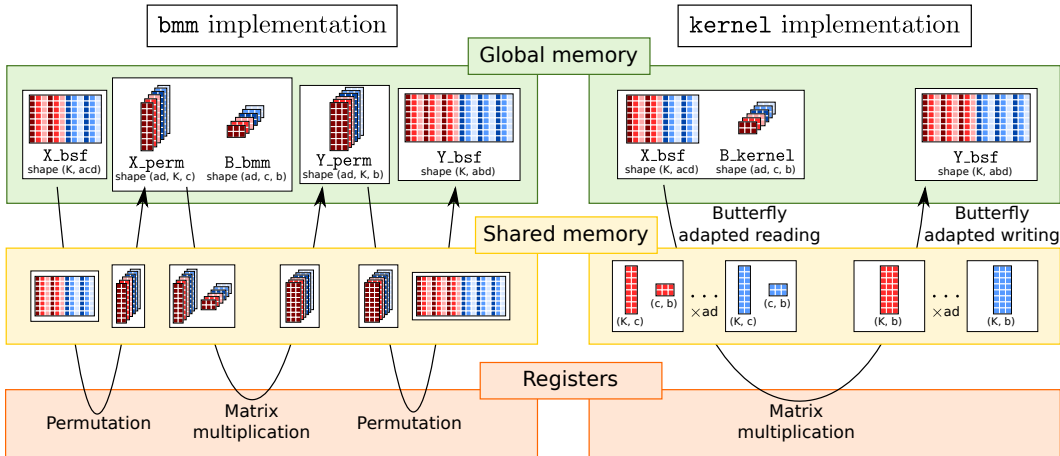


Figure 4: Data flow between the different levels of GPU memory for the `bmm` implementation (Section 2.2) from Dao et al. [2022b] and the new `kernel` (Section 4).

<sup>6</sup>By analogy with the recent PyTorch optimization channels last that moves the channels dimension to the last position for convolutional layers.

Let us focus on `bmm`, as we will find it to be faster than `einsum` and `bsr`. The data flow of `bmm` is illustrated in Figure 4. There is one pass between the global memory and the registers to perform the permutation with  $\mathbf{P}$  (line 3 in Algorithm 2), one for the multiplication with  $\tilde{\mathbf{B}}$  (line 2), and another one for the permutation with  $\mathbf{Q}$  (line 1).

Doing at least three passes between the global memory and the registers is necessary for any implementation that performs all the multiplications  $\mathbf{X}[:, \text{col}]\mathbf{B}^\top[\text{col}, \text{row}]$  (line 5 in Algorithm 1, or equivalently line 2 in Algorithm 2) by calling high-performance libraries from common Python interfaces (PyTorch, Tensorflow). Indeed, calling multiplication routines from Python requires in general having the entries of  $\mathbf{X}[:, \text{col}]$  and  $\mathbf{B}^\top[\text{col}, \text{row}]$  stored contiguously in *global memory*. This is not the case of the entries of  $\mathbf{X}[:, \text{col}]$  when  $\mathbf{X} \in \mathbb{R}^{K \times N}$  is directly stored contiguously in a 2D-tensor of shape  $(K, N)$  or  $(N, K)$ , and when  $d > 1$ , because the indices in `col` are equally spaced by  $d$  (see line 4 in Algorithm 2). And this is the only memory layout that we can assume for the entries of  $\mathbf{X}$  when the matrix multiplication is a part of a larger pipeline, such as in a neural network. Therefore, a first pass between the global memory and the registers is required to write the entries of  $\mathbf{X}[:, \text{col}]$  contiguously in global memory, see Figure 4. Similarly, the result of the multiplication  $\mathbf{Y}[:, \text{row}] = \mathbf{X}[:, \text{col}]\mathbf{B}^\top[\text{col}, \text{row}]$ , as returned by an efficient routine called from Python, will in general be stored contiguously in *global memory* for each pair  $(\text{row}, \text{col})$ . But indices in `row` are equally spaced by  $d$ : this requires another pass to rewrite them equally spaced by  $d$  in the *final* output 2D-tensor storing all the entries of  $\mathbf{Y}$  contiguously in memory. With the pass implied by the actual multiplication routine, this results in three passes between the global memory and the registers (Figure 4).

**Estimated time for memory rewritings in `bmm`.** To the best of our knowledge, this paper is the first to discuss the practical cost of memory rewritings in baseline implementations such as `bmm`. For input and output dimensions  $N$  and  $M$ , and a batch size  $K$ , the memory rewritings of  $\mathbf{X}[:, \text{col}]$  and  $\mathbf{Y}[:, \text{row}]$  for all pairs  $(\text{row}, \text{col})$  (Algorithm 1) concern  $KN + KM$  coefficients to be moved in memory: each coefficient of the input and output tensors is moved exactly once. The total number of scalar multiplications performed when computing the products  $\mathbf{Y}[:, \text{row}] = \mathbf{X}[:, \text{col}]\mathbf{B}^\top[\text{col}, \text{row}]$  for all  $(\text{row}, \text{col})$  (Algorithm 1) is equal to  $K \times \text{\#nnz}$  (batch size times the number of nonzero in  $\mathbf{B}$ ).

Figure 5 reports time estimates for memory rewritings in the `bmm` implementation (see Appendix B.2 for more details on the experimental protocol). It shows that the relative time spent on memory rewritings increases with the ratio

$$\frac{\text{number of memory rewritings}}{\text{number of scalar multiplications}} = \frac{KN + KM}{K \times \text{\#nnz}} = \frac{b + c}{bc} \quad (2)$$

where the last equality holds in the case of a butterfly factor with sparsity pattern  $\pi = (a, b, c, d)$ , since  $N = acd$ ,  $M = abd$  and  $\text{\#nnz} = abcd$  in this case. Figure 5 shows that **these memory rewritings can take up to 45% of the total runtime**.<sup>7</sup> In conclusion, *it is crucial to optimize the data transfers between the different levels of GPU memory to improve current implementations.*

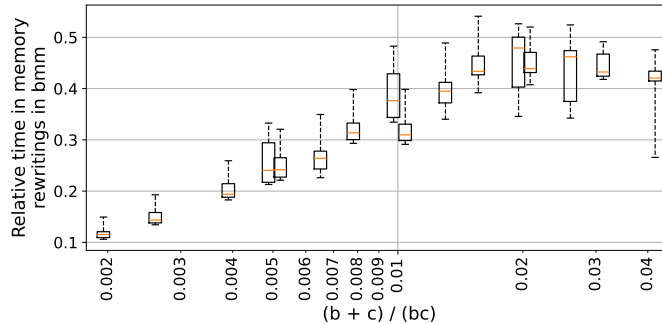


Figure 5: Estimated relative time spent on memory rewritings in `bmm` for the multiplication with  $\mathbf{B} \in \Sigma^\pi$ , for several  $\pi = (a, b, c, d)$ . We regroup patterns by their value of  $(b + c)/(bc)$ , and plot a boxplot to summarize the corresponding measurements.

<sup>7</sup>Regardless of the memory layout convention, *batch-size-first* or *batch-size-last*.

## 4 New CUDA kernel with reduced memory transfers

For better management of memory accesses, we need to go to a lower level than Python. This is where the new CUDA kernel comes in. It has the minimum possible number of back and forth between global memory and registers thanks to custom read and write phases between global and shared memory, tailored to *butterfly sparsity*. These new read and write phases allow to perform a *single* back and forth between the different levels of memory, as shown in Figure 4.

**Implementation.** The reading phase loads the entries of  $\mathbf{X}[:, \text{col}]$  directly from the global memory by accessing *non-contiguous* columns of  $\mathbf{X}$  equally spaced by  $d$  (see Figure 3), and stores them *contiguously* in shared memory. Since we are still loading entire columns of  $\mathbf{X}$ , the reading phase is expected to be more efficient if the entries in the same column are contiguous in memory, in order to ensure that most of the memory accesses remain contiguous and efficient. This will only be the case when  $\mathbf{X}$  is stored with the *batch-size-last* memory layout (as defined in Section 2.2). When in shared memory, the kernel implements the classic tile matrix multiplication algorithm<sup>8</sup> [Li et al., 2019, Boehm, 2022, NVIDIA, 2023a,b, 2024] to compute each product  $\mathbf{X}[:, \text{col}]\mathbf{B}^\top[\text{col}, \text{row}]$  for each subsets  $\text{row}, \text{col}$  in Algorithm 1. Once these products are computed, the kernel again has a custom writing phase from shared to global memory, rewriting the results that are stored contiguously in shared memory, to non-contiguous locations in global memory, because each submatrix  $\mathbf{Y}[:, \text{row}]$  corresponds to non-consecutive columns of the output  $\mathbf{Y}$  (see Figure 3). This writing phase is also expected to be more efficient in the *batch-size-last* memory layout, ensuring the entries of a same column of  $\mathbf{Y}[:, \text{row}]$ , and thus the write operations, to be contiguous in memory.

**Comparison with other baseline implementations.** This new kernel has fewer global memory accesses compared to the baselines `einsum`, `bsr` and `bmm`, because it only reads each coefficient of  $\mathbf{X}$  and  $\mathbf{B}$  once and writes the result of the multiplication  $\mathbf{Y}$  once, while those baseline implementations read  $\mathbf{X}$  and  $\mathbf{Y}$  twice and rewrite them once (to permute them). It also has fewer global memory accesses compared to the dense implementation (Section 2.2), since the dense implementation also reads the *zero* entries of  $\mathbf{B}$  and the corresponding coefficients of  $\mathbf{X}$ , while our kernel does not. Compared to the generic sparse implementation, we have the same number of memory accesses, but the sparse implementation is agnostic to the sparsity structure of  $\mathbf{B}$ , so it is expected to be less efficient since the memory accesses are not tailored to the known location of the nonzero entries.

## 5 Benchmarking the multiplication by a single butterfly factor

We perform the first benchmark of different implementations for butterfly matrix multiplication, at the finest granularity, where we measure the time for the multiplication with a *single* butterfly factor  $\mathbf{B}$ . In particular, we validate numerically the benefits of reducing the memory transfers in the `kernel` implementation, compared to the baselines `einsum`, `bsr` and `bmm`.

**Protocol.** The benchmark is run in *float-precision* on a subset of 600 sparsity patterns  $\pi = (a, b, c, d)$  in  $\alpha \times \beta \times \beta \times \alpha$ , with  $\alpha := \{1, 2, 3, 4, 6, 8, 12, 16, 24, 32, 48, 64, 96, 128\}$ ,  $\beta := \{48, 64, 96, 128, 192, 256, 384, 512, 768, 1024\}$ , such that  $b = c$  or  $b = 4c$  or  $c = 4b$ . These patterns correspond to dimensions of butterfly factors  $\mathbf{B} \in \mathbb{R}^{M \times N}$  with  $(M, N) = (abd, acd)$  that could be used in neural networks. We choose as batch size  $K = 128 \times 196 = 25088$ , which is standard as it corresponds to the effective batch size for linear layers in ViTs where the number of sequences per batch is 128, and the number of tokens per sequence is 196. Further details are given in Appendix B.1.

**Implementations specialized to butterfly sparsity improves over generic implementations.** The first line of Table 2 shows that at least one of the implementations specialized to the butterfly structure among `kernel`, `bmm`, `einsum` and `bsr` improves over the generic dense and sparse implementation, which do not take into account the butterfly sparsity. The speedup increases with the matrix size, see Appendix B.3.

**The baseline `bmm` is faster than the other baselines `einsum` and `bsr`.** This is shown in the second line of Table 2, where the `bmm` implementation improves over  $\min(\text{einsum}, \text{bsr})$  in 93% of the tested cases. The speedup increases with the matrix size, see Appendix B.4. Therefore, when comparing

<sup>8</sup>Classical optimizations are used, as detailed in Appendix D.2.



Table 2: Percentage out of 600 patterns  $(a, b, c, d)$  where `algo1` is *faster* than the `algo2` (denoted by  $\text{time}(\text{algo1}) < \text{time}(\text{algo2})$ ), and the median acceleration factor in such cases (that is, the median ratio  $\frac{\text{time of algo2}}{\text{time of algo1}}$ ). For each implementation, we take the minimum time between the *batch-size-first* and the *batch-size-last* memory layout.

$\min \text{time} \begin{pmatrix} \text{kernel} \\ \text{bmm} \\ \text{einsum} \\ \text{bsr} \end{pmatrix} < \min \text{time} \begin{pmatrix} \text{dense} \\ \text{sparse} \end{pmatrix}$	$\text{time}(\text{bmm}) < \min \text{time} \begin{pmatrix} \text{einsum} \\ \text{bsr} \\ \text{dense} \\ \text{sparse} \end{pmatrix}$	$\text{time}(\text{kernel}) < \min \text{time} \begin{pmatrix} \text{bmm} \\ \text{einsum} \\ \text{bsr} \\ \text{dense} \\ \text{sparse} \end{pmatrix}$
99.67% ( $\times 6.57$ )	92.66% ( $\times 1.37$ )	88.10% ( $\times 1.39$ )

the new `kernel` implementation to other baselines, we will mainly focus on the comparison between `bmm` and `kernel`.

**The new kernel implementation is faster than existing baselines.** The third row of Table 2 shows that `kernel` is faster than all other baselines in 88% of the tested patterns. This empirically validates the benefits of the reduced memory transfer in the `kernel` implementation. In the following, we provide further details on the influence of the memory layout (*batch-size-first* vs. *batch-size-last*) on this improvement. Additionally, we analyze the patterns  $\pi = (a, b, c, d)$  for which the `kernel` outperforms baseline implementations.

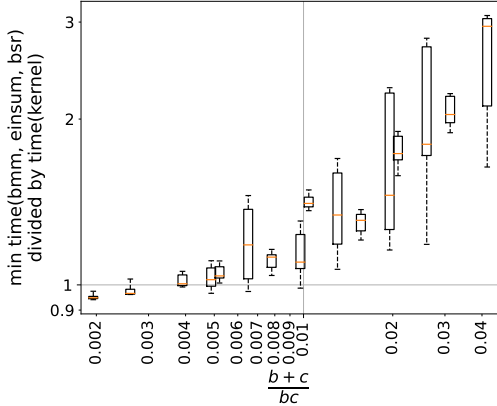


Figure 6: Time speedup factor of `kernel` compared to  $\min(\text{bmm}, \text{einsum}, \text{bsr})$ . For each implementation, we take the minimum time between the *batch-size-first* and *batch-size-last* memory layouts. We regroup the patterns by their value of  $(b+c)/(bc)$ , and plot a boxplot to summarize the corresponding measurements.

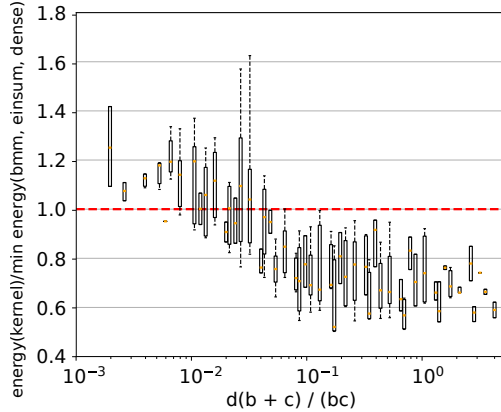


Figure 7: Energy consumed by `kernel` compared to the minimum consumed by `bmm`, `einsum` and `bsr`. For each implementation, we take the minimum energy consumed between the *batch-size-first* and *batch-size-last* memory layouts. We regroup patterns by their value of  $d(b+c)/(bc)$ .

**Impact of the memory layout.** For baseline implementations, switching to *batch-size-last* yields a high systematic speedup for `sparse`, high variability in the speedup of `bsr`, and essentially no impact to negative impact for the other methods, see Appendix B.5 for numerical results. The important part is that it has no impact on `bmm`, and since `bmm` is the fastest baseline implementation (Table 2), switching to *batch-size-last* has no impact on the best of the baseline implementations. However, it yields a systematic speedup (about  $\times 2$ ) for the `kernel` implementation. This acceleration is expected, since the *batch-size-last* memory layout allows for more efficient memory accesses in the `kernel` implementation, as detailed in Section 4.

**Analyzing the cases where `kernel` outperforms baselines.** As seen in Section 4, the `kernel` has an improved memory access design compared to the rest of the baselines. Figure 6 confirms this experimentally: **the kernel implementation becomes increasingly time-efficient compared to the baseline implementations as the relative number of memory accesses increases**, i.e. when the

following ratio increases (introduced in (2))

$$\frac{\text{number of memory rewritings}}{\text{number of scalar multiplications}} = (b + c)/(bc).$$

**The kernel improves on energy efficiency.** For sparsity patterns  $\pi = (a, b, c, d)$ , the integer  $d$  corresponds to the distance between two columns of the butterfly factor with the same set of nonzero entries. When  $d$  is large, the memory rewritings made by `bmm` are likely to be more expensive as the columns in the same set `col` of Algorithm 1 are further away from each other. In practice, we observe the `kernel` to be more and more energy-efficient as the relative number of memory rewritings  $(b + c)/bc$  times the cost  $d$  of these memory rewritings increases, as shown in Figure 7. Overall, the median energy reduction factor is  $\times 0.85$ , and the new kernel improves the energy consumption in 72% of the tested cases. See Appendix B.1 for details about the measurements. This is particularly noteworthy as it demonstrates that **the kernel not only achieves higher time efficiency but also reduces energy consumption** compared to other baselines. This dual advantage makes the `kernel` an effective solution for improving both performance and sustainability.

## 6 Broader implications for neural networks: accelerating inference

The inference of neural networks is claimed to represent 90% of the cost of machine learning at scale according to independent reports from both NVIDIA [HPCwire, 2019] and Amazon Web Services [Jeff Barr, 2019]. We now investigate whether replacing fully-connected layers by butterfly matrices accelerates the inference. While the same could also apply to other architectures, we will consider Vision Transformers (ViTs) [Dosovitskiy et al., 2020]. We find that the computational cost of fully-connected layers is significant in such architectures: depending on the size of the ViT, from 30% to 60% of the total time in a forward pass is spent in fully-connected layers (see Appendix B.6 for details).

**Protocol.** We benchmark in *float-precision* various components of a ViT-S/16 architecture: a linear layer with bias, an MLP with non-linear activation and/or normalization layers, a multi-head attention module, etc. As in Dao et al. [2022b], the matrices that are replaced by a butterfly matrix are the weight matrices of linear layers in feed-forward network modules, and the projection matrices for keys, queries and values in multi-head attention modules. We focus on *batch-size-first* as it is the default convention in PyTorch<sup>9</sup>. Details and some additional results are given in Appendix B.7.

**Results.** We denote by `time(fully-connected)` the inference time without butterfly matrices (and therefore, with the standard PyTorch implementation). Table 3 shows that `time(kernel) < time(bmm) < time(fully-connected)` over all the different submodules. **This concretely shows that using butterfly matrices and the kernel implementation accelerates the inference of standard neural networks.**

Table 3: Acceleration of submodules of a ViT-S/16 using butterfly matrices.

	$\frac{\text{time(bmm)}}{\text{time(fully-connected)}}$	$\frac{\text{time(kernel)}}{\text{time(fully-connected)}}$
Linear $N \times N$	0.82	<b>0.50</b>
Feed-forward network	0.91	<b>0.77</b>
Multi-head attention	0.87	<b>0.79</b>
Block	0.90	<b>0.78</b>
Butterfly ViT-S/16	0.89	<b>0.78</b>

## 7 Conclusion

This work is the first to evaluate the efficiency of existing butterfly sparse matrix multiplication algorithms on the GPU. Our benchmark shows that baseline implementations require costly memory rewrites in global memory, which are not negligible in practice. The proposed new CUDA kernel significantly reduces the cost of global memory accesses. Specifically, this new kernel is faster than

<sup>9</sup>The insertion of butterfly matrices in the *batch-size-last* memory layout would *a priori* require a careful implementation of the rest of the operations, that are for now optimized in *batch-size-first* in PyTorch.

previous baseline implementations, with a median reduction factor of  $\times 0.85$ . We also show how it can be used to accelerate the inference of neural networks.

**Perspectives.** While we have focused on optimizing memory management, the multiplication part of our kernel may still have room for improvement, especially in *half-precision*. We hope this will encourage work in that direction. The new kernel is particularly performant in *batch-size-last*. We hope this will lead to further efforts in the *batch-size-first* setting and encourage revisiting other common operations in neural networks within the *batch-size-last* configuration. A translation of our kernel into OpenCL could enable it to run on AMD hardware and other platforms. We also hope that our benchmark will serve as a baseline for comparing butterfly implementations on other hardware: CPU, Intelligence Processing Unit, FPGA, etc.

## Acknowledgments

This work was supported in part by the AllegroAssai ANR-19-CHIA-0009, by the NuSCAP ANR-20-CE48-0014 projects of the French Agence Nationale de la Recherche and by the SHARP ANR project ANR-23-PEIA-0008 in the context of the France 2030 program.

The authors thank the Blaise Pascal Center for the computational means. It uses the SIDUS [Quemener and Corvellec, 2013] solution developed by Emmanuel Quemener.

We would also like to thank Patrick Pérez, Gilles Puy, Elisa Riccietti, Nicolas Brisebarre, and Rémi Gribonval for their useful feedback, and Emmanuel Quemener for reserving computing resources for us while we ran our experiments.

## References

- Simon Boehm. How to optimize a CUDA matmul kernel for cuBLAS-like performance: A worklog, 2022. <https://siboehm.com/articles/22/CUDA-MMM> [Accessed: April 2024].
- Tri Dao, Albert Gu, Matthew Eichhorn, Atri Rudra, and Christopher Ré. Learning fast algorithms for linear transforms using butterfly factorizations. In *ICML*, 2019.
- Tri Dao, Beidi Chen, Kaizhao Liang, Jiaming Yang, Zhao Song, Atri Rudra, and Christopher Re. Pixelated butterfly: Simple and efficient sparse training for neural network models. In *ICLR*, 2022a.
- Tri Dao, Beidi Chen, Nimit S Sohoni, Arjun Desai, Michael Poli, Jessica Grogan, Alexander Liu, Aniruddh Rao, Atri Rudra, and Christopher Ré. Monarch: Expressive structured matrices for efficient and accurate training. In *ICML*, 2022b.
- Tri Dao, Dan Fu, Stefano Ermon, Atri Rudra, and Christopher Ré. Flashattention: Fast and memory-efficient exact attention with io-awareness. *Advances in Neural Information Processing Systems*, 35:16344–16359, 2022c.
- Alexey Dosovitskiy, Lucas Beyer, Alexander Kolesnikov, Dirk Weissenborn, Xiaohua Zhai, Thomas Unterthiner, Mostafa Dehghani, Matthias Minderer, Georg Heigold, Sylvain Gelly, et al. An image is worth 16x16 words: Transformers for image recognition at scale. In *ICLR*, 2020.
- Daniel Y Fu, Simran Arora, Jessica Grogan, Isys Johnson, Sabri Eyuboglu, Armin W Thomas, Benjamin Spector, Michael Poli, Atri Rudra, and Christopher Ré. Monarch mixer: A simple sub-quadratic GEMM-based architecture. In *NeurIPS*, 2023.
- Rémi Gribonval, Theo Mary, and Elisa Riccietti. Optimal quantization of rank-one matrices in floating-point arithmetic—with applications to butterfly factorizations. preprint, 2023. URL <https://inria.hal.science/hal-04125381>.
- HPCwire. AWS Upgrades its GPU-Backed AI Inference Platform. <https://www.hpcwire.com/2019/03/19/aws-upgrades-its-gpu-backed-ai-inference-platform/>, March 2019. Accessed: [April 2024].
- Jeff Barr. Amazon EC2 Update – Inf1 Instances with AWS Inferentia Chips for High Performance Cost-Effective Inferencing. [aws.amazon.com/blogs/aws/amazon-ec2-update-inf1-instances-with-aws-inferentia-chips-for-high-performance-cost-effective-inferencing](https://aws.amazon.com/blogs/aws/amazon-ec2-update-inf1-instances-with-aws-inferentia-chips-for-high-performance-cost-effective-inferencing), 2019. Accessed: [April 2024].

- Quoc-Tung Le. *Algorithmic and theoretical aspects of sparse deep neural networks*. PhD thesis, 2023. URL <https://inria.hal.science/tel-04329531>.
- Quoc-Tung Le, Léon Zheng, Elisa Riccietti, and Rémi Gribonval. Fast learning of fast transforms, with guarantees. In *ICASSP*, 2022.
- Xiuhong Li, Yun Liang, Shengen Yan, Liancheng Jia, and Yinghan Li. A coordinated tiling and batching framework for efficient GEMM on GPUs. In *Proceedings of the 24th Symposium on Principles and Practice of Parallel Programming*, 2019.
- Rui Lin, Jie Ran, King Hung Chiu, Graziano Chesi, and Ngai Wong. Deformable butterfly: A highly structured and sparse linear transform. In *NeurIPS*, 2021.
- NVIDIA. Efficient GEMM in CUDA: documentation, 2023a. [https://github.com/NVIDIA/cutlass/blob/main/media/docs/efficient\\_gemm.md](https://github.com/NVIDIA/cutlass/blob/main/media/docs/efficient_gemm.md) [Accessed: April 2024].
- NVIDIA. Matrix multiplication background user’s guide, 2023b. <https://docs.nvidia.com/deeplearning/performance/dl-performance-matrix-multiplication/index.html> [Accessed: April 2024].
- NVIDIA. CUDA C++ programming guide, 2024. <https://docs.nvidia.com/cuda/cuda-c-programming-guide/index.html> [Accessed: April 2024].
- E. Quemener and M. Corvellec. SIDUS—the Solution for Extreme Deduplication of an Operating System. *Linux Journal*, 2013.
- Alex Rogozhnikov. Einops: Clear and reliable tensor manipulations with einstein-like notation. In *ICLR*, 2021.
- Keivan Alizadeh Vahid, Anish Prabhu, Ali Farhadi, and Mohammad Rastegari. Butterfly transform: An efficient FFT based neural architecture design. In *CVPR*, 2020.
- Charles F Van Loan. The ubiquitous kronecker product. *Journal of computational and applied mathematics*, 123(1-2):85–100, 2000.
- Phil Wang. Scaled dot-product attention implementation, 2024a. <https://docs.nvidia.com/deeplearning/performance/dl-performance-matrix-multiplication/index.html> [Accessed: April 2024].
- Phil Wang. Simple ViT implementation, 2024b. [https://github.com/lucidrains/vit-pytorch/blob/main/vit\\_pytorch/simple\\_vit.py](https://github.com/lucidrains/vit-pytorch/blob/main/vit_pytorch/simple_vit.py) [Accessed: April 2024].
- Xiaohua Zhai, Alexander Kolesnikov, Neil Houlsby, and Lucas Beyer. Scaling vision transformers. In *CVPR*, 2022.
- Léon Zheng, Elisa Riccietti, and Rémi Gribonval. Efficient identification of butterfly sparse matrix factorizations. *SIAM Journal on Mathematics of Data Science*, 5(1):22–49, 2023.

# Appendices

## A Related works

We now review the numerical results we found in the literature about time efficiency of existing algorithms for sparse butterfly matrix multiplication.

It is reported in Dao et al. [2022b] that some butterfly networks were twice faster to train than their dense counterparts for image classification and language modeling, without additional information.

In Fu et al. [2023] is reported an acceleration of  $\mathbf{X} \mapsto \mathbf{W}^{-1}(\mathbf{K} \odot \mathbf{W}\mathbf{X})$  where  $\mathbf{K}$  is some dense weight matrix,  $\odot$  is the element-wise multiplication, and  $\mathbf{W}$  is the DFT matrix (which admits a butterfly factorization), as soon as the dimensions of  $\mathbf{W}$  are at least equal to 4096.

These results do not provide *extensive* information on the efficiency of sparse butterfly matrix multiplication, motivating the benchmark in this paper.

## B Experiments

### B.1 Details on the experiments

The pytorch package version is 2.2 and pytorch-cuda is 12.1.

**Matrix sizes.** In all our experiments with matrices, we set the batch size to  $K = 128 \times 196 = 25088$ , a very standard choice for ViTs, as this quantity corresponds to the standard number of tokens per sequence (192) multiplied by the standard number of sequences in a batch of inputs (128). When dealing with a batch of images in neural networks, we choose the standard choice of batch size  $K = 128$ .

**Matrix entries.** The coordinates of any butterfly factor  $\mathbf{B} \in \mathbb{R}^{abd \times acd}$  with sparsity pattern  $(a, b, c, d)$  are drawn i.i.d. uniformly in  $[-\frac{1}{\sqrt{c}}, \frac{1}{\sqrt{c}}]$ , as for the initialization chosen for training in Dao et al. [2022b], while the coordinates of the inputs  $\mathbf{X}$  are drawn i.i.d. according to a standard normal distribution  $\mathcal{N}(0, 1)$ .

**Benchmarking time execution.** All the experiments measuring the time execution of the implementations (Tables 2, 3, 4 and 7, Figures 5 to 6 and 9 to 17) are done on a single NVIDIA A100-PCIE-40GB GPU on an Intel(R) Xeon(R) Silver 4215R CPU @ 3.20GHz with 377G of memory. The full benchmark took approximately 3 days in an isolated environment, ensuring that no other processes were running concurrently.

Measurements are done using the PyTorch tool `torch.utils.benchmark.Timer`. The medians are computed on at least 10 measurements of 10 runs. In 94.2% of the cases, we have an interquartile range (IQR) that is at least 100 times smaller than the median (resp. 98% for 50 times smaller, and 99.7% for 10 times smaller).

**Benchmarking energy consumption.** Measurements of the energy consumption (Figure 7) is done on a single NVIDIA Tesla V100-PCIE-16GB GPU on an Intel(R) Xeon(R) Silver 4215R CPU @ 3.20GHz with 754G of memory. The full benchmark took approximately 1.5 days in an isolated environment. Measurements are made using the pyJoules software toolkit. The medians are computed on at 10 measurements of at least 16 runs. In 96% of the cases, the IQR is at least 10 times smaller than the median, and in all the cases, it is 5 times smaller.

**Patterns benchmarked for time measurements (Section 5).** The considered patterns are generated by the Python code written in Figure 8. In all the cases, we only consider patterns  $(a, b, c, d)$  with  $b = c$  or  $b = 4c$  or  $c = 4d$  to have an input size  $N$  and an output size  $M$  such that  $N = M$  or  $N = 4M$  or  $M = 4N$ . This choice is motivated by the fact that fully-connected layers in ViTs satisfy have input and output sizes satisfying these constraints.

The first "for" loop in Figure 8 generates a wide range of patterns  $(a, b, c, d)$  with  $a = 1$ , as this represents the simplest scenario. Indeed, the case  $a > 1$  simply corresponds to the case  $a = 1$  but repeated  $a$  times in parallel.

The second "for" loop in Figure 8 generates patterns with  $a > 1$  offering fewer choices for  $d$  to keep the benchmark concise in terms of execution time. This loop also imposes additional conditions on  $b$  and  $c$  (line 28 of the code) that we now explain. Many graphs are plotted based on the ratio  $(b + c)/bc$ , as introduced in Equation (2). Because of that, our goal was to include as many distinct ratios  $(b + c)/bc$  as possible while keeping the benchmark brief. We excluded certain  $(b, c)$  values because they resulted in a ratio that was very close to one already in the benchmark and were more computationally intensive.

```

1 import itertools
2
3 batch_size = 25_088
4 size_limit = 2_147_483_647
5
6 a_list = [1, 2, 3, 4, 6, 8, 12, 16, 24, 32, 48, 64, 96, 128]
7 b_list = [48, 64, 96, 128, 192, 256, 384, 512, 768, 1024]
8 c_list = [48, 64, 96, 128, 192, 256, 384, 512, 768, 1024]
9 d_list1 = [1, 2, 3, 4, 6, 8, 12, 16, 24, 32, 48, 64, 96, 128]
10 d_list2 = [4, 16, 64]
11
12 def get_patterns_benchmark():
13     patterns_list = []
14
15     def add_pattern(a, b, c, d):
16         if batch_size * a * c * d <= size_limit and \
17             batch_size * a * b * d <= size_limit and \
18             a * b * c * d <= size_limit:
19             patterns_list.append((a, b, c, d))
20
21     for b, c, d in itertools.product(b_list, c_list, d_list1):
22         a = 1
23         if (b == c or b == 4 * c or c == 4 * b):
24             add_pattern(a, b, c, d)
25
26     for a, b, c, d in itertools.product(a_list, b_list, c_list,
27                                         d_list2):
28         if a != 1 and \
29             (b, c) not in [(1024, 256), (256, 1024), (128, 512), (512,
30                             128), (64, 256), (256, 64)] and \
31             (b == c or b == 4 * c or c == 4 * b):
32             add_pattern(a, b, c, d)
33
34     return patterns_list

```

Figure 8: Python code to generate the patterns benchmarked for the execution time in the numerical experiments of Section 5.

**Patterns benchmarked for energy measurements (Section 5).** For the energy measurements, the goal is to have diverse sparsity patterns  $(a, b, c, d)$  corresponding to many different ratios  $d(b + c)/bc$  to observe the trend in Figure 7, while keeping the benchmark as short as possible. We chose to consider the cartesian product of

```

1 a_list = [1, 4, 16, 32, 64]
2 b_list = [48, 64, 96, 128, 192, 256, 384, 512, 768, 1024]
3 c_list = [48, 64, 96, 128, 192, 256, 384, 512, 768, 1024]
4 d_list = [1, 2, 3, 4, 6, 8, 12, 16, 24, 32, 48, 64]

```

by skipping as in Figure 8 all the patterns with

```

1 (b, c) in [(1024, 256), (256, 1024), (128, 512), (512, 128),
2            (64, 256), (256, 64)]

```

and also all the patterns such that

```
1 b != c and b != 4 * c and c != 4 * b
```

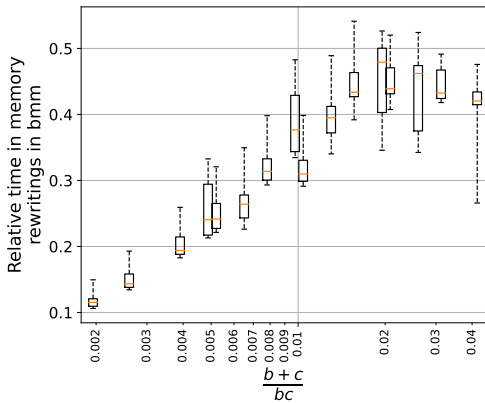
for the same reasons as the ones explained above in the case of the benchmark on the time execution.

**Details on boxplots.** In all boxplots (Figures 5 to 7 and 9 to 17), the orange line corresponds to the median, the boxes to the first and third quartile and the whiskers to the 5th and the 95th percentile. Outliers are not represented on the graph.

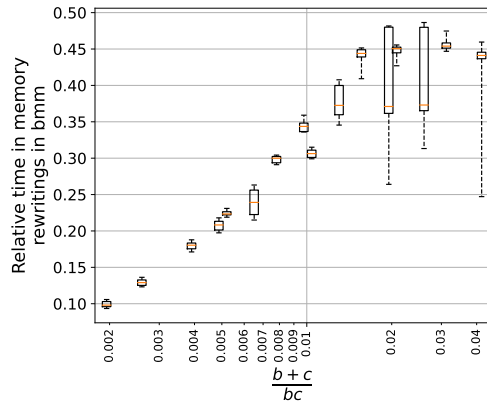
## B.2 Estimating the time for memory rewritings in the `bmm` implementation (Section 3)

**Protocol.** Given a pattern  $\pi = (a, b, c, d)$  and an input  $\mathbf{X} \in \mathbb{R}^{K \times acd}$  for some batch size  $K$ , we first measure the time  $\Delta t$  to compute  $\mathbf{Y} := \mathbf{X}\mathbf{B}^\top$  using the `bmm` implementation. Then, we measure the time  $\Delta \hat{t}$  to perform only the multiplication operations  $\mathbf{Y}[:, \text{row}] = \mathbf{X}[:, \text{col}]\mathbf{B}^\top[\text{col}, \text{row}]$  in the `bmm` implementation (line 2 of Algorithm 2). Therefore, the estimated relative time to perform the memory rewritings of lines 1 and 3 of Algorithm 2 is simply  $\frac{\Delta t - \Delta \hat{t}}{\Delta t}$ .

**Results.** Figure 5, which is replicated in the left part of Figure 9, shows that the relative time spent doing memory rewritings in `bmm` increases with the ratio  $(b+c)/(bc)$ , in the *batch-size-first* memory layout. Figure 9 shows that this is similar for both *batch-size-first* and *batch-size-last*.



(a) Batch-size-first (same as Figure 5).



(b) Batch-size-last.

Figure 9: Estimated relative time spent on memory rewritings in `bmm` for the multiplication with  $\mathbf{B} \in \Sigma^\pi$ , for several  $\pi = (a, b, c, d)$ . We regroup patterns by their value of  $(b+c)/(bc)$ , and plot a boxplot to summarize the corresponding measurements.

## B.3 Details on `min time(kernel, bmm, bsr, einsum)` vs. `min time(dense, sparse)` (Section 5)

Figure 10 shows that the speed-up factor of implementations specialized to the butterfly sparsity (`kernel`, `bmm`, `bsr`, `einsum`) over the generic `dense` and `sparse` implementations increases with the matrix size  $M \times N$ . We recall that  $M = acd$  and  $N = abd$  for a butterfly factor with pattern  $\pi = (a, b, c, d)$ .

## B.4 Details on `time(bmm)` vs. `min time(bsr, einsum)` (Section 5)

Figure 11 shows that for a sufficient large matrix size  $M \times N$ , we always have `time(bmm) < min time(bsr, einsum)`, i.e., the `bmm` implementation is the most efficient among all baseline implementations (`bmm`, `einsum`, `bsr`).

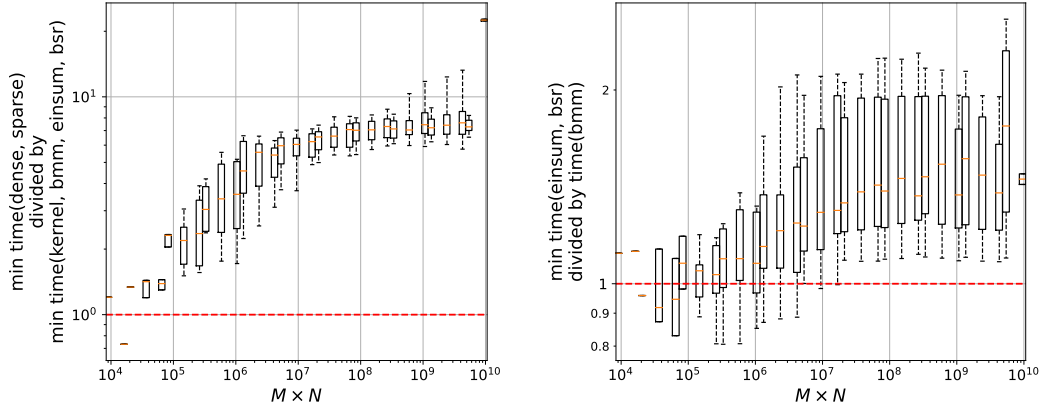


Figure 10: Speed-up factor of  $\min(\text{time}(\text{kernel}, \text{bmm}, \text{einsum}, \text{bsr}))$  compared to  $\min(\text{time}(\text{dense}, \text{sparse}))$  as a function of the matrix size  $M \times N$ . Figure 11: Speed-up factor of  $\text{time}(\text{bmm})$  compared to  $\min(\text{time}(\text{einsum}, \text{bsr}))$  as a function of the matrix size  $M \times N$ .

### B.5 Details on the impact of the memory layout (Section 5)

Figure 12 shows the impact of the memory layout on the execution time of each implementation.

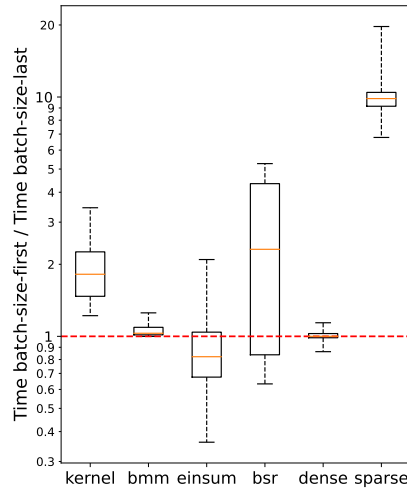


Figure 12: Boxplots of the ratio  $\frac{\text{time of batch-size-first}}{\text{time of batch-size-last}}$ .

Table 4 shows the percentage of patterns for which the `kernel` implementation improves over all baseline implementations, either in the *batch-size-first* or the *batch-size-last* memory layout. When restricting all implementations to the *batch-size-first* layout, the `kernel` still improves on 20% of the tested patterns despite non-contiguous memory accesses (Section 4).

Table 4: Percentage out of 600 patterns ( $a, b, c, d$ ) where `algo1` is faster than the `algo2` (denoted by  $\text{time}(\text{algo1}) < \text{time}(\text{algo2})$ ), and the median acceleration factor in such cases (that is, the median ratio  $\frac{\text{time of algo2}}{\text{time of algo1}}$ ).

	$\text{time}(\text{kernel}) < \min(\text{time}(\text{bmm}, \text{einsum}, \text{bsr}, \text{dense}, \text{sparse}))$
<i>Batch-size-first</i>	20.0% ( $\times 1.28$ )
<i>Batch-size-last</i>	88.1% ( $\times 1.39$ )



## B.6 Time spent in linear layers in vision transformers

This section gives a numerical lower bound estimate on the time spent in fully-connected layers in a Vision Transformer (ViT).

**Results.** Table 5 shows that, for different ViTs, the fraction of computation time solely dedicated to linear layers in feed-forward network modules varies between 31% and 53% in *half-precision*, and 46% and 61% in *float-precision*. This proportion increases with the size of the architecture. This shows that a non-negligible amount of ViTs inference is dedicated to fully-connected layers. Note that the time for the fully-connected linear layers in the multi-head attention module is not included in our measurements, so our estimate is *only a lower bound* on the time effectively devoted to all fully-connected layers in transformer architectures.

Table 5: Median execution times (ms) of the forward pass in a ViT, and the forward pass in an MLP containing only all the linear layers involved in the feed-forward network modules of the ViT. The latter is reported with its ratio over the first. FP16 is *half-precision*, FP32 is *float-precision*.

ARCHITECTURE	FP16 (S)		FP32 (S)	
	COMPLETE	LINEAR IN FFNS	COMPLETE	LINEAR IN FFNS
ViT-S/16	0.014	0.0046 (31%)	0.090	0.04 (46%)
ViT-B/16	0.036	0.015 (42%)	0.30	0.16 (54%)
ViT-L/16	0.11	0.050 (46%)	1.0	0.58 (58%)
ViT-H/14	0.31	0.16 (53%)	2.6	1.6 (61%)

**Details on the estimation.** The transformer architecture is composed of a sequence of transformer blocks, where each block contains a multi-head attention module and a feed-forward network module. The feed-forward network module is an MLP with one hidden layer of neurons, involving two fully-connected linear layers. Table 5 reports the time to perform sequentially all the fully-connected linear layers (without biases) appearing in feed-forward network modules of the considered ViT. This is compared to the total forward time of the transformer network. This is expected to yield a lower bound since we did not measure the time spent in fully-connected linear layers in the multi-head attention module.

**Experimental settings.** The architecture ViT-S/16 corresponds to the one in Zhai et al. [2022], while the architecture ViT-B/16, ViT-L/16 and ViT-H/14 correspond to those in Dosovitskiy et al. [2020]. Input images are of size  $224 \times 224$ . In *float-precision*, the PyTorch implementation of ViT architecture are taken from Wang [2024b]. In *half-precision*, the considered implementation of the transformer architecture uses FlashAttention Dao et al. [2022c] to compute the scaled dot product attention, like in Wang [2024a]. The MLP containing only the linear layers of the feed-forward modules in the transformer architecture is implemented using `torch.nn.Sequential` and `torch.nn.Linear`. Experiments are done on a single A100-40GB GPU on AMD EPYC 7742 64-Core Processor. Measurements are done using the PyTorch tool `torch.utils.benchmark.Timer` for benchmarking. The image batch size is set at 128.

## B.7 Details on the acceleration of the inference of a ViT (Section 6)

**Chosen butterfly matrices.** The weight matrices are replaced by butterfly matrices associated to the following butterfly architectures of depth 2 (Definition 2.1):  $(1, 192, 48, 2)$ ,  $(2, 48, 192, 1)$  for the size  $N \times N$ ,  $(1, 768, 192, 2)$ ,  $(6, 64, 64, 1)$  for the size  $4N \times N$ ,  $(1, 768, 192, 2)$ ,  $(6, 64, 64, 1)$  for the size  $4N \times N$ .

**Additional results.** Table 6 provides additional results to Table 3 on linear submodules of a ViT-S/16.

Table 6: Acceleration of submodules of a ViT-S/16 using butterfly matrices.

	$\frac{\text{time}(\text{bmm})}{\text{time}(\text{fully-connected})}$	$\frac{\text{time}(\text{kernel})}{\text{time}(\text{fully-connected})}$
Linear $N \times N$	0.82	<b>0.50</b>
Linear $N \times N + \text{bias}$	0.97	<b>0.66</b>
Linear $4N \times N$	0.80	<b>0.78</b>
Linear $4N \times N + \text{bias}$	0.93	<b>0.90</b>
Linear $N \times 4N$	0.91	<b>0.58</b>
Linear $N \times 4N + \text{bias}$	0.94	<b>0.61</b>

### B.8 Additional results in half-precision

For the sake of completeness we perform the benchmark described in Section 5 in *half-precision*. The equivalent of Table 2, Figure 6, Figures 9 to 12 in *half-precision* are Table 7, Figure 13, Figures 14 to 17, respectively. Note that just as Figure 6, the Figure 13 only considers sparsity patterns for which  $\min \text{time}(\text{kernel}, \text{bmm}, \text{bsr}, \text{einsum}) < \min \text{time}(\text{dense}, \text{sparse})$ . This corresponds to 87% of the tested patterns in *half-precision*, cf. Table 7.

Table 7: Percentage out of 600 patterns ( $a, b, c, d$ ) where algo1 is *faster* than the algo2 in *half-precision* (denoted by  $\text{time}(\text{algo1}) < \text{time}(\text{algo2})$ ), and the median acceleration factor in such cases (that is, the median ratio  $\frac{\text{time of algo2}}{\text{time of algo1}}$ ). For each implementation, we take the minimum time between the *batch-size-first* and the *batch-size-last* memory layout. Experiments are carried in *half-precision*.

$\min \text{time} \begin{pmatrix} \text{kernel} \\ \text{bmm} \\ \text{einsum} \\ \text{bsr} \end{pmatrix} < \min \text{time} \begin{pmatrix} \text{dense} \\ \text{sparse} \end{pmatrix}$	$\text{time}(\text{bmm}) < \min \text{time} \begin{pmatrix} \text{einsum} \\ \text{bsr} \\ \text{dense} \\ \text{sparse} \end{pmatrix}$	$\text{time}(\text{kernel}) < \min \text{time} \begin{pmatrix} \text{bmm} \\ \text{einsum} \\ \text{bsr} \\ \text{dense} \\ \text{sparse} \end{pmatrix}$
86.95% ( $\times 8.45$ )	83.22% ( $\times 1.83$ )	36.69% ( $\times 1.46$ )

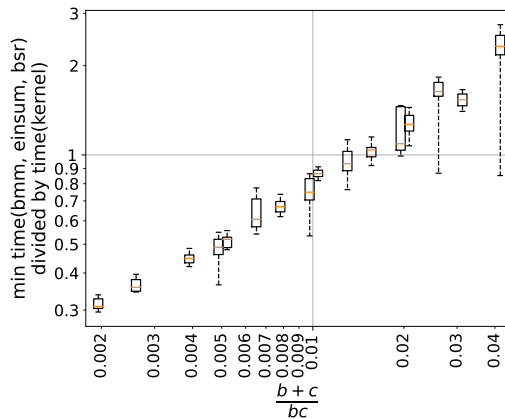


Figure 13: Speedup factor of kernel compared to  $\min(\text{bmm}, \text{einsum}, \text{bsr})$  in *half-precision*. For each implementation, we take the minimum time between the *batch-size-first* and the *batch-size-last* memory layout. We regroup the ( $a, b, c, d$ ) patterns by their value of  $(b+c)/(bc)$ , and use a boxplot to summarize the corresponding measurements. Experiments are carried in *half-precision*.

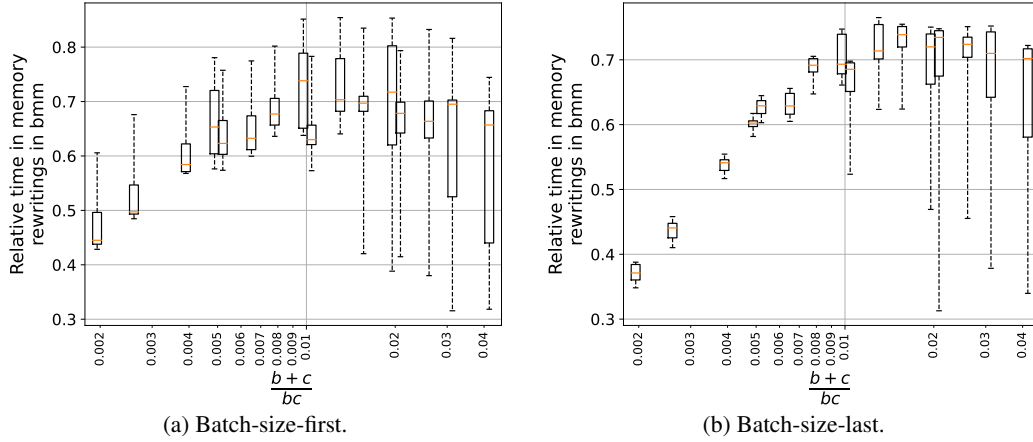


Figure 14: Estimated relative time spent on memory rewritings in `bmm` for the multiplication with  $\mathbf{B} \in \Sigma^\pi$ , for several  $\pi = (a, b, c, d)$ . We regroup patterns by their value of  $(b+c)/(bc)$ , and plot a boxplot to summarize the corresponding measurements. Experiments are carried in *half-precision*.

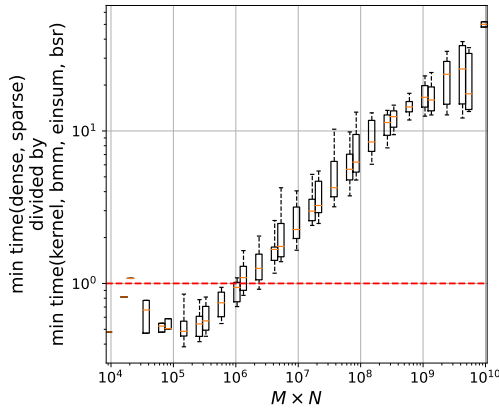


Figure 15: Speed-up factor of `min time(kernel, bmm, einsum, bsr)` compared to `min time(dense, sparse)` vs. the matrix size  $M \times N$ . Experiments are carried in *half-precision*.

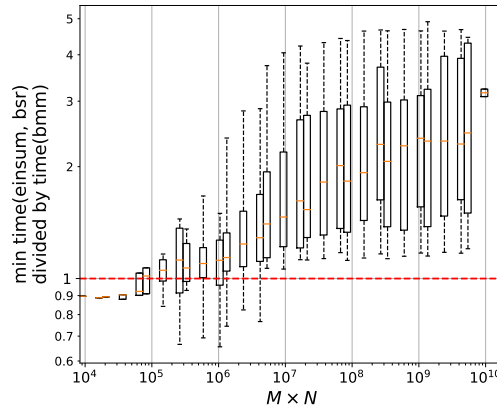


Figure 16: Speed-up factor of `time(bmm)` compared to `min time(einsum, bsr)` vs. the matrix size  $M \times N$ . Experiments are carried in *half-precision*.

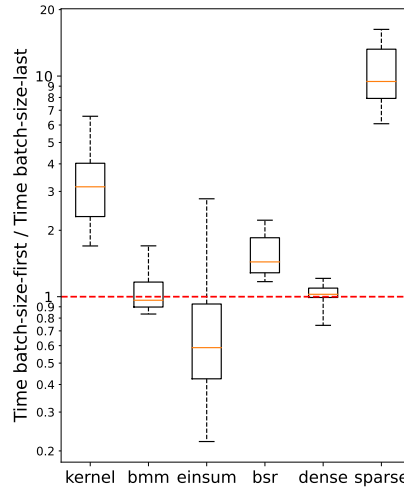


Figure 17: Boxplots of the ratio  $\frac{\text{time of batch-size-first}}{\text{time of batch-size-last}}$  in *half-precision*.

## C Theoretical results

### C.1 Details on perfect shuffle permutations

The goal is to prove Equation (1), which we recall here for convenience:

$$\mathbf{S}_\pi = \underbrace{(\mathbf{I}_a \otimes \mathbf{P}_{b,d})}_{:=\mathbf{P}} \underbrace{(\mathbf{I}_{ad} \otimes \mathbf{1}_{b \times c})}_{:=\mathbf{S}_\pi} \underbrace{(\mathbf{I}_a \otimes \mathbf{P}_{c,d})^\top}_{:=\mathbf{Q}},$$

where the matrix  $\mathbf{P}_{p,q}$  is the so-called  $(p, q)$  perfect shuffle permutation introduced below. To prove this formula, we will use the next lemma.

**Lemma C.1.** *For any positive integers  $b, c, d$ :*

$$\mathbf{P}_{b,d}^\top (\mathbf{1}_{b \times c} \otimes \mathbf{I}_d) \mathbf{P}_{c,d} = \mathbf{I}_d \otimes \mathbf{1}_{b \times c},$$

where  $\mathbf{P}_{p,q}$  denotes the  $(p, q)$  perfect shuffle of  $r := pq$  [Van Loan, 2000], which is the permutation matrix of size  $r \times r$  defined as:

$$\mathbf{P}_{p,q} := \begin{pmatrix} \mathbf{I}_r[R_0, :] \\ \mathbf{I}_r[R_1, :] \\ \vdots \\ \mathbf{I}_r[R_{q-1}, :] \end{pmatrix}, \quad (3)$$

where  $R_i := \{i + qj \mid j \in \llbracket 0, p-1 \rrbracket\}$  for  $i \in \llbracket 0, q-1 \rrbracket$ .

*Proof of Lemma C.1.* This is a direct consequence of a more general result claiming that the Kronecker product commutes up to some perfect shuffle permutation matrices [Van Loan, 2000, Section 1].  $\square$

We now turn to the proof of Equation (1).

*Proof of Equation (1).* By definition,  $\mathbf{S}_\pi = \mathbf{I}_a \otimes \mathbf{1}_{b \times c} \otimes \mathbf{I}_d$  when  $\pi = (a, b, c, d)$ . By Lemma C.1,

$$\mathbf{S}_\pi = \mathbf{I}_a \otimes \mathbf{1}_{b \times c} \otimes \mathbf{I}_d = \mathbf{I}_a \otimes \left( \mathbf{P}_{b,d} (\mathbf{I}_d \otimes \mathbf{1}_{b \times c}) \mathbf{P}_{c,d}^\top \right).$$

By the equality  $(\mathbf{A}\mathbf{B}) \otimes (\mathbf{C}\mathbf{D}) = (\mathbf{A} \otimes \mathbf{C})(\mathbf{B} \otimes \mathbf{D})$  for any matrices  $\mathbf{A}, \mathbf{B}, \mathbf{C}, \mathbf{D}$  of compatible sizes, we get the result:

$$\begin{aligned} \mathbf{S}_\pi &= \mathbf{I}_a \otimes \left( \mathbf{P}_{b,d} (\mathbf{I}_d \otimes \mathbf{1}_{b \times c}) \mathbf{P}_{c,d}^\top \right) \\ &= (\mathbf{I}_a \otimes \mathbf{P}_{b,d}) \left( \mathbf{I}_a \otimes \left( (\mathbf{I}_d \otimes \mathbf{1}_{b \times c}) \mathbf{P}_{c,d}^\top \right) \right) \\ &= (\mathbf{I}_a \otimes \mathbf{P}_{b,d}) (\mathbf{I}_a \otimes \mathbf{I}_d \otimes \mathbf{1}_{b \times c}) (\mathbf{I}_a \otimes \mathbf{P}_{c,d}^\top) \\ &= (\mathbf{I}_a \otimes \mathbf{P}_{b,d}) (\mathbf{I}_{ad} \otimes \mathbf{1}_{b \times c}) (\mathbf{I}_a \otimes \mathbf{P}_{c,d}^\top). \end{aligned}$$

$\square$

### C.2 Existing variants of butterfly factorization

Table 8 summarizes how Definition 2.1 [Lin et al., 2021, Le, 2023] captures all the variants of butterfly factorizations that have been empirically tested for deep neural networks in the literature Dao et al. [2019, 2022a,b], Vahid et al. [2020], Lin et al. [2021], Fu et al. [2023]. Note that the butterfly chain that we consider from Dao et al. [2022b] is the one used in their actual implementation rather than in their paper. A detailed explanation about this unification can be found in Chapter 6 of Le [2023], except for the case of block butterfly Dao et al. [2022a]. We now deal with the latter: we explain why block butterfly matrices are indeed covered by Definition 2.1.

#### Block butterfly matrices are covered by Definition 2.1.

Block butterfly factors [Dao et al., 2022a] are a direct generalization of square dyadic butterfly factors [Dao et al., 2019]. Indeed, replacing each entry of a square dyadic butterfly factor by a block matrix of size  $t \times t$  gives a block butterfly factor (and in particular, the square dyadic butterfly factors are

Table 8: Definition 2.1 unifies the different factorizations tested for deep neural networks in the literature, as documented in Lin et al. [2021], Le [2023]. The fact that it also captures block butterfly matrices is new (Appendix C.2).

	MATRIX SIZE	BUTTERFLY ARCHITECTURE
DENSE	$M \times N$	$(1, M, N, 1)$
LOW-RANK	$M \times N$	$(1, M, r, 1), (1, r, N, 1)$
SQUARE DYADIC [DAO ET AL., 2019, VAHID ET AL., 2020]	$N \times N$ WITH $N = 2^L$	$(2^{\ell-1}, 2, 2, 2^{L-\ell})_{\ell=1}^L$
KALEIDOSCOPE [DAO ET AL., 2022B]	$N \times N$ WITH $N = 2^L$	CONCATENATE $(2^{\ell-1}, 2, 2, 2^{L-\ell})_{\ell=1}^L$ AND $(2^{L-\ell}, 2, 2, 2^{\ell-1})_{\ell=1}^L$
BLOCK BUTTERFLY [DAO ET AL., 2022A]	$N \times N$ WITH $N = 2^{Lt}$	$(2^{\ell-1}, 2t, 2t, 2^{L-\ell})_{\ell=1}^L$
MONARCH [DAO ET AL., 2022B, FU ET AL., 2023]	$M \times N$	$(1, M/p, \min(M, N)/p, p), (p, \min(M, N)/p, N/p, 1)$
DEFORMABLE BUTTERFLY [LIN ET AL., 2021]	INTRODUCED THE GENERAL FRAMEWORK OF DEFINITION 2.1.	

particular cases of block butterfly factors with block size  $1 \times 1$ .) The support constraints of block butterfly factors can be expressed by the following binary matrix [Dao et al., 2022a]:

$$\tilde{\mathbf{S}}_{\ell} := \mathbf{I}_{2^{\ell-1}} \otimes \mathbf{1}_{2 \times 2} \otimes \mathbf{I}_{2^{L-\ell}} \otimes \mathbf{1}_{t \times t}, \quad \ell = 1, \dots, L, \quad (4)$$

where we have an additional parameter  $t$  in comparison to the tuples of butterfly factors (Definition 2.1) to control the block size.

We argue that using a chain of block butterfly factors (4) is equivalent to using a chain of butterfly factors in the sense of Definition 2.1. In order to prove that, we first introduce the set of matrices that can be factorized according to the two alternative definitions.

**Definition C.2** (Set of block butterfly matrices). Consider the chain of  $L$  block butterfly factors of block size  $t$ , define  $\mathcal{B}_b^{L,t} := \{\prod_{\ell=1, \dots, L} \mathbf{X}_{\ell} \mid \text{supp}(\mathbf{X}_{\ell}) \subseteq \text{supp}(\tilde{\mathbf{S}}_{\ell})\}$  ( $\tilde{\mathbf{S}}_{\ell}$  is defined as in (4)) the set of matrix admitting an exact factorization into block butterfly factors (shortened to block butterfly matrices).

**Definition C.3** (Set of butterfly matrices associated to a butterfly chain  $\Theta := (\mathbf{t}_{\ell})_{\ell=1}^L$ ). Consider a butterfly chain  $\Theta := (\mathbf{t}_{\ell})_{\ell=1}^L$ , we define  $\mathcal{B}^{\Theta} := \{\prod_{\ell=1, \dots, L} \mathbf{X}_{\ell} \mid \text{supp}(\mathbf{X}_{\ell}) \subseteq \text{supp}(\mathbf{S}_{\mathbf{t}_{\ell}})\}$  the set of matrix admitting an exact factorization into butterfly factors (shortened to butterfly matrices).

The equivalence between block butterfly factors and butterfly chain is shown in the following lemma:

**Lemma C.4.** Consider  $\Theta := (\mathbf{t}_{\ell})_{\ell=1}^L$  where  $\mathbf{t}_{\ell} := (2^{\ell-1}, 2t, 2t, 2^{L-\ell})$ ,  $\ell = 1, \dots, L$ ,  $\Theta$  is equivalent to the chain of  $L$  block butterfly factors of block size  $t$  in the sense that there exists two permutation matrices  $(\mathbf{P}, \mathbf{Q})$  of size  $2^L t \times 2^L t$  such that:

$$\mathcal{B}_b^{L,t} = \mathbf{P} \mathcal{B}^{\Theta} \mathbf{Q} := \{\mathbf{P} \mathbf{B} \mathbf{Q} \mid \mathbf{B} \in \mathcal{B}^{\Theta}\}.$$

In words, the two sets  $\mathcal{B}_b^{L,t}$  and  $\mathcal{B}^{\Theta}$  are *expressively equivalent* up to permutation of rows and columns.

*Proof of Lemma C.4.* Consider the permutation matrices:

$$\mathbf{P}_{\ell} := \mathbf{I}_{2^{\ell-1}} \otimes \mathbf{T}_{\ell} \quad \mathbf{Q}_{\ell} := \mathbf{I}_{2^{\ell}} \otimes \mathbf{T}_{\ell+1}^{\top}, \quad \ell = 1, \dots, L, \quad (5)$$

where  $\mathbf{T}_{\ell}$  (whose size is  $2^{L-\ell+1} t \times 2^{L-\ell+1} t$ ) is the permutation matrix corresponding to the permutation:

$$(1, t+1, \dots, (2^{L-\ell+1} - 1)t + 1, 2, t+2, \dots, (2^{L-\ell+1} - 1)t + 2, \dots, t, 2t, \dots, 2^{L-\ell+1} t).$$

The proof relies on the following claim:

$$\mathbf{P}_{\ell} \tilde{\mathbf{S}}_{\ell} \mathbf{Q}_{\ell} = \mathbf{S}_{\mathbf{t}_{\ell}}, \quad \forall \ell = 1, \dots, L, \quad (6)$$

which means that applying  $\mathbf{P}$ ,  $\mathbf{Q}$  to the left and right of the  $\ell$ th block butterfly factors turn it into a  $\mathbf{t}_{\ell}$ -butterfly factors. Before proving (6), we explain how we can finish the proof of Lemma C.4 based on (6). Firstly, to prove the inclusion  $\mathcal{B}_b^{L,t} \subseteq \mathbf{P}_1^{\top} \mathcal{B}^{\Theta} \mathbf{Q}_1^{\top}$ , observe that:

$$\mathbf{Q}_{\ell-1} \mathbf{P}_{\ell} = (\mathbf{I}_{2^{\ell}} \otimes \mathbf{T}_{\ell}^{\top})(\mathbf{I}_{2^{\ell-1}} \otimes \mathbf{T}_{\ell}) = \mathbf{I}_{2^{\ell-1}} \otimes (\mathbf{T}_{\ell}^{\top} \mathbf{T}_{\ell}) = \mathbf{I}_{2^{\ell-1}} \otimes \mathbf{I}_{2^{L-\ell+1} t} = \mathbf{I}_{2^L t}, \quad (7)$$

where we use the identity  $(\mathbf{A} \otimes \mathbf{B})(\mathbf{C} \otimes \mathbf{D}) = (\mathbf{AC}) \otimes (\mathbf{BD})$  (applicable only when the matrix multiplication  $\mathbf{AC}$  and  $\mathbf{BD}$  is well-defined) and  $\mathbf{PP}^\top = \mathbf{I}$  for any permutation matrix. Thus, consider  $(\tilde{\mathbf{X}}_\ell)_{\ell=1,\dots,L}$  a sequence of  $L$  block butterfly factors of block size  $t$ , we have:

$$\begin{aligned} \tilde{\mathbf{X}}_1 \tilde{\mathbf{X}}_2 \dots \tilde{\mathbf{X}}_L &\stackrel{(7)}{=} (\mathbf{P}_1^\top \mathbf{P}_1) \tilde{\mathbf{X}}_1 (\mathbf{Q}_1 \mathbf{P}_2) \tilde{\mathbf{X}}_2 \dots (\mathbf{Q}_{L-1} \mathbf{P}_L) \tilde{\mathbf{X}}_L (\mathbf{Q}_L \mathbf{Q}_L^\top) \\ &\stackrel{(6)}{=} \mathbf{P}_1^\top \underbrace{(\mathbf{P}_1 \tilde{\mathbf{X}}_1 \mathbf{Q}_1)}_{t_1\text{-butterfly factor}} \underbrace{(\mathbf{P}_2 \tilde{\mathbf{X}}_2 \mathbf{Q}_2)}_{t_2\text{-butterfly factor}} \dots \underbrace{(\mathbf{P}_L \tilde{\mathbf{X}}_L \mathbf{Q}_L)}_{t_L\text{-butterfly factor}} \mathbf{Q}_L^\top \in \mathbf{P}_1^\top \mathcal{B}^\Theta \mathbf{Q}_L^\top. \end{aligned}$$

Therefore,  $\mathcal{B}_b^{L,t} \subseteq \mathbf{P}_1^\top \mathcal{B}^\Theta \mathbf{Q}_L^\top$ . Secondly, to see the other inclusion, from (6), we also have:

$$\mathbf{S}_\ell^b = \mathbf{P}_\ell^\top \mathbf{S}_{t_\ell} \mathbf{Q}_\ell^\top, \quad \forall \ell = 1, \dots, L. \quad (8)$$

Similar to the proof of  $\mathcal{B}_b^{L,t} \subseteq \mathbf{P}_1^\top \mathcal{B}^\Theta \mathbf{Q}_L^\top$ , we can consider  $(\mathbf{X}_\ell)_{\ell=1,\dots,L}$  where  $\mathbf{X}_\ell$  is a  $t_\ell$ -butterfly factor. We have:

$$\begin{aligned} \mathbf{P}_1^\top \mathbf{X}_1 \mathbf{X}_2 \dots \mathbf{X}_L \mathbf{Q}_L^\top &\stackrel{(7)}{=} \mathbf{P}_1^\top \mathbf{X}_1 (\mathbf{P}_2 \mathbf{Q}_1)^\top \mathbf{X}_2 \dots \mathbf{X}_{L-1} (\mathbf{P}_L \mathbf{Q}_{L-1})^\top \mathbf{X}_L \mathbf{Q}_L^\top \\ &\stackrel{(8)}{=} \underbrace{(\mathbf{P}_1^\top \mathbf{X}_1 \mathbf{Q}_1^\top)}_{1\text{st block butterfly factor}} \dots \underbrace{(\mathbf{P}_L^\top \mathbf{X}_L \mathbf{Q}_L^\top)}_{L\text{th block butterfly factor}} \in \mathcal{B}_b^{L,t}. \end{aligned}$$

Thus,  $\mathbf{P}_1^\top \mathcal{B}^\Theta \mathbf{Q}_L^\top \subseteq \mathcal{B}_b^{L,t}$ . We can conclude that  $\mathbf{P}_1^\top \mathcal{B}^\Theta \mathbf{Q}_L^\top = \mathcal{B}_b^{L,t}$  and the pair of permutation matrices  $(\mathbf{P}_1^\top, \mathbf{Q}_L^\top)$  satisfies Lemma C.4.

Finally, it remains to prove (6). Using the identity:  $(\mathbf{A}_1 \otimes \dots \otimes \mathbf{A}_n)(\mathbf{B}_1 \otimes \dots \otimes \mathbf{B}_n)(\mathbf{C}_1 \otimes \dots \otimes \mathbf{C}_n) = (\mathbf{A}_1 \mathbf{B}_1 \mathbf{C}_1) \otimes \dots \otimes (\mathbf{A}_n \mathbf{B}_n \mathbf{C}_n)$  (when  $\mathbf{A}_\ell \mathbf{B}_\ell \mathbf{C}_\ell$ ,  $\ell = 1, \dots, n$  makes sense), we have:

$$\begin{aligned} \mathbf{P}_\ell \mathbf{S}_\ell^b \mathbf{Q}_\ell &= (\mathbf{I}_{2^{\ell-1}} \otimes \mathbf{T}_\ell) (\mathbf{I}_{2^{\ell-1}} \otimes \mathbf{1}_{2 \times 2} \otimes \mathbf{I}_{2^{L-\ell}} \otimes \mathbf{1}_{t \times t}) (\mathbf{I}_{2^\ell} \otimes \mathbf{T}_{\ell+1}^\top) \\ &= \mathbf{I}_{2^{\ell-1}} \otimes [\mathbf{T}_\ell (\mathbf{1}_{2 \times 2} \otimes \mathbf{I}_{2^{L-\ell}} \otimes \mathbf{1}_{t \times t}) (\mathbf{I}_2 \otimes \mathbf{T}_{\ell+1}^\top)], \forall \ell = 1, \dots, L. \end{aligned}$$

Thus, it is sufficient to prove that:

$$\mathbf{T}_\ell (\mathbf{1}_{2 \times 2} \otimes \mathbf{I}_{2^{L-\ell}} \otimes \mathbf{1}_{t \times t}) (\mathbf{I}_2 \otimes \mathbf{T}_{\ell+1}^\top) = \mathbf{1}_{2t \times 2t} \otimes \mathbf{I}_{2^{L-\ell}}, \forall \ell = 1, \dots, L.$$

To show the equation above, we will use an ad-hoc argument. Note that the binary matrix  $\mathbf{1}_{2 \times 2} \otimes \mathbf{I}_{2^{L-\ell}} \otimes \mathbf{1}_{t \times t}$  has exactly  $2^{L-\ell}$  different columns (resp. rows). If we partition them into  $2^{L-\ell}$  groups  $\{1, \dots, 2^{L-\ell}\}$  and label each of them by the partition they belong to, then the columns and rows will have the form:

$$\underbrace{(1, \dots, 1)}_{t \text{ times}}, \underbrace{(2, \dots, 2)}_{t \text{ times}}, \dots, \underbrace{(2^{L-\ell}, \dots, 2^{L-\ell})}_{t \text{ times}}, \underbrace{(1, \dots, 1)}_{t \text{ times}}, \underbrace{(2, \dots, 2)}_{t \text{ times}}, \dots, \underbrace{(2^{L-\ell}, \dots, 2^{L-\ell})}_{t \text{ times}}.$$

This procedure of labeling can be visualized as in Figure 18 for a simple case where  $L - \ell = 1$  and  $t = 3$ . To turn  $\mathbf{1}_{2 \times 2} \otimes \mathbf{I}_{2^{L-\ell}} \otimes \mathbf{1}_{t \times t}$  into  $\mathbf{1}_{2t \times 2t} \otimes \mathbf{I}_{2^{L-\ell}}$ , the permutation matrices on the left and right (in this case,  $\mathbf{T}_\ell$  and  $\mathbf{I}_2 \otimes \mathbf{T}_{\ell+1}^\top$ ) need to permute the columns and rows such that the label becomes:

$$\underbrace{(1, 2, \dots, 2^{L-\ell})}_{1\text{st}}, \underbrace{(1, 2, \dots, 2^{L-\ell})}_{2\text{nd}}, \dots, \underbrace{(1, 2, \dots, 2^{L-\ell})}_{2\text{tth}}.$$

It can be seen directly that  $\mathbf{T}_\ell$  permutes the label of the rows correctly. For  $\mathbf{I}_2 \otimes \mathbf{T}_{\ell+1}^\top$ , this permutation matrix permutes the columns in the first half and the second half separately (due to the Kronecker product with  $\mathbf{I}_2$ ) and each half is permuted by the permutation described in (5). Thanks to this interpretation, it can be seen that  $\mathbf{I}_2 \otimes \mathbf{T}_{\ell+1}^\top$  also permutes the label of the columns correctly as well. This concludes the proof.  $\square$

## D Implementations

### D.1 Details on baseline GPU implementations

To keep it short, we only give the code in the case of the *batch-size-first* memory layout (except for dense and sparse where the codes are small). The case of *batch-size-last* can simply be obtained by inverting the first and last positions in all tensor reshapings.

**einsum implementation.** This implementation uses tensor contractions with the high-performance einops library. The *abcd* nonzero entries of the butterfly factor  $\mathbf{B}$  (Figure 2) are stored in a PyTorch 4D-tensor  $\mathbf{B\_einsum}$  of shape  $(a, b, c, d)$ . The implementation uses Einstein notations.

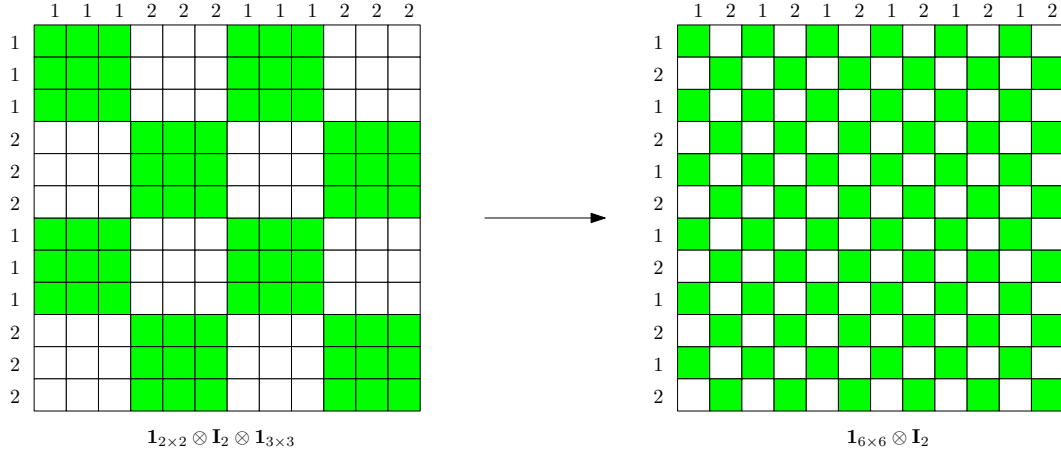


Figure 18: Illustration for the proof of (6). Green and white squares represent the 1s and 0s of the binary matrices respectively.

```

1 def butterfly_einsum(X_bsf, B_einsum):
2     X_perm = einops.rearrange(X_bsf, "... (a c d) -> ... a c d", a=a,
3     c=c, d=d)
4     Y_perm = einops.einsum(X_perm, B_einsum, "... a c d, a b c d ->
5     ... a b d")
6     Y_bsf = einops.rearrange(Y_perm, "... a b d-> ... (a b d)")
7     return Y_bsf

```

The second line of this code does at the same time all the matrix multiplications  $\mathbf{Y}[:, \text{row}] \leftarrow \mathbf{X}[:, \text{col}] \mathbf{B}^\top[\text{col}, \text{row}]$  for all the pairs (row, col) in Algorithm 1.

**bsr implementation.** This is an implementation of Algorithm 2 using the high-performance Block compressed Sparse Row (BSR) PyTorch library. The matrix  $\tilde{\mathbf{B}}$  is stored as a tensor  $\mathbf{B\_bsr}$  stored in the BSR format.

```

1 def butterfly_bsr(X_bsf, B_bsr):
2     batch_size = X_bsf.shape[0]
3     X_perm = (
4         X_bsf.view(batch_size, a, c, d)
5         .transpose(-1, -2)
6         .reshape(batch_size, a * c * d)
7     )
8     Y_perm = torch.nn.functional.linear(
9         X_perm, B_bsr
10    )
11    Y_bsf = (
12        Y_perm.view(batch_size, a, d, b)
13        .transpose(-1, -2)
14        .reshape(batch_size, a * b * d)
15    )
16    return Y_bsf

```

**bmm implementation.** This is an implementation of Algorithm 2 using the high-performance Block compressed Sparse Row (BSR) PyTorch library. The matrix  $\tilde{\mathbf{B}}$  is stored as a tensor  $\mathbf{B\_bsr}$  stored in the BSR format. This implementation using `torch.bmm`, which is based on high-performance batched matrix multiplication NVIDIA routines. The non-zero entries of  $\tilde{\mathbf{B}}$  are stored in a four-dimensional PyTorch tensor  $\mathbf{B\_bmm}$  of shape  $(a * d, b, c)$ .

```

1 def butterfly_bmm(X_bsf, B_bmm):
2     batch_size = X_bsf.shape[0]
3     X_perm = (

```

```

4         X_bsf.view(batch_size, a, c, d)
5         .transpose(-1, -2)
6         .reshape(batch_size, a * d, c).
7         contiguous().
8         transpose(0, 1)
9     )
10    Y_perm = torch.empty(batch_size, a * d, b, device=x.device, dtype=
        x.dtype).transpose(0, 1)
11    Y_perm = torch.bmm(X_perm, B_bmm.transpose(-1, -2))
12    Y_bsf = (
13        Y_perm.transpose(0, 1)
14        .reshape(batch_size, a, d, b)
15        .transpose(-1, -2)
16        .reshape(batch_size, a * b * d)
17    )
18    return

```

**dense implementation.** This ignores the sparsity of the butterfly factor  $\mathbf{B}$ , that is stored as a dense matrix in a 2d-tensor  $B_{\text{dense}}$ .

*batch-size-first:* `torch.nn.functional.linear(X_bsf, B_dense)`

*batch-size-last:* `torch.matmul(B_dense, X_bsf)`

The implementation in *batch-size-first* is the default PyTorch implementation of a forward pass of a linear layer. For *batch-size-last*, we had to choose an implementation since Pytorch uses *batch-size-first* by default. We made our choice based on a small benchmark of different alternatives.

**sparse implementation.** This exploits the sparsity of the butterfly factor  $\mathbf{B}$  but not its structure (recall that the support are not arbitrary, they are structured since they must be expressed as Kronecker products, see Definition 2.1).

*batch-size-first:* `torch.nn.functional.linear(X_bsf, B_csr)`

*batch-size-last:* `torch.matmul(B_csr, X_bsf)`

## D.2 Details on the kernel implementation

**Classical optimizations that we build upon.** The proposed implementation use *vectorization* as soon as an operation can be vectorized. Concretely, the float4 and half2 vector types are used to mutualize read/write operations [NVIDIA, 2023b,a, 2024, Boehm, 2022]. An *epilogue* [NVIDIA, 2023a] is also implemented to avoid writing in global memory in a disorganized way. Indeed, after having accumulated the output in registers, each thread has specific rows and columns of the output to write to global memory, and may finish its computation before the others. To avoid that, the epilogue starts to write in the shared memory, in a disorganized way, and then organize the writing from shared to global memory. Another implemented optimization is *double buffering* NVIDIA [2023b,a], Boehm [2022], Li et al. [2019]: a thread block is always both computing the output of a tile, and loading the next tile from global to shared memory. This allows us to hide some latency that arises when loading from the global memory.

Note that as with any CUDA kernel, the constants (such as the number of threads) need to be tailored to each specific case of use —here, each butterfly sparsity pattern  $\pi = (a, b, c, d)$ — and to each GPU.